THE PROCEEDINGS OF
THE PHYSICAL SOCIETY

Section A

VOL. 62, PART 4 | 1 April 1949 | No. 352 A

# The Performance of Infra-Red Spectrometers as Limited by Detector Characteristics

BY E. F. DALY AND G. B. B. M. SUTHERLAND
Pembroke College, Cambridge

*MS. received 11th June 1948*

*ABSTRACT.* The performance of the average infra-red spectrometer is conditioned mainly by the characteristics of the detector employed. Assuming a minimum usable energy level at the exit slit, the square of the minimum frequency band embraced by the exit slit is proportional to the minimum energy level and to the focal length of the collimator, and inversely proportional to the angular dispersion of the prism or grating, the area of the collimator mirror, the energy flux at the entrance slit and the slit length. If, however, the time of response of the detector is taken into account, the inter-relation of spectrum scanning speed, signal-to-noise ratio and resolving power must be considered. For this purpose a simplified model of an infra-red detector has been used, defined by three parameters. This allows the relative merits of detectors to be assessed and the performance of any given spectrometer with a specified detector to be estimated. The inter-relation of resolving power and spectral scanning speed has been examined for " chopped-beam " and " video " presentation.

## §1. INTRODUCTION

DURING the past ten years several new detectors of infra-red radiation have been developed which are superior to the older ones in speed and sensitivity. The general characteristics of these have been reviewed (Sutherland and Lee 1948, Williams 1948) and some applications have been made in the spectroscopic field, e.g. to achieve cathode-ray presentation of spectra (Daly and Sutherland 1947) or higher resolution of complex spectra (Sutherland, Blackwell and Fellgett 1946), but it is important to enquire into the conditions under which these various detectors may best be used in spectroscopy. If the optimum performance is to be obtained from a spectrometer designed to use one of these detectors it is necessary to investigate carefully the inter-relations between scanning speed, resolving power and detector characteristics. This in turn leads to a consideration of the best way in which to define the characteristics of a detector which is being used for spectroscopic purposes.

In general the resolving power obtainable with an infra-red spectrometer is limited by the performance of the detector and not by the usual optical criteria. We propose therefore to introduce the term "separating power" to indicate the minimum frequency band which can be embraced by the exit slit for a given ratio of the signal produced by the detector to the inherent noise. It will then be the speed with which a spectrum can be scanned for a given separating power which determines the performance of a spectrometer. We start by considering how separating power is related to the optical constants of the spectrometer, working above the limits imposed by aberration and diffraction but employing the specified

minimum usable power input of the detector and ignoring its speed of response. We next consider how this minimum power level is related to the speed of response of the detector, the detector noise and the scanning speed for a given signal-to-noise ratio at the display. In order to do so, however, it is desirable first to define the characteristics of the detector in terms of three parameters, viz. $\sigma$ the responsivity (say in microvolts per microwatt) when the full signal has been reached, $\tau$ the time constant (time to reach $1/e$ of the full signal) and $\mu$, inherent noise of the detector. Finally the complex inter-relations between scanning speed and separating power are derived in graphical form for various detectors operating in a spectrometer of specified design.

## § 2. MODEL SPECTROMETER

The spectrometer design employed as the basis for discussion is shown in Figure 1. Assuming a small plane black-body source, the power $W_\nu$ in the

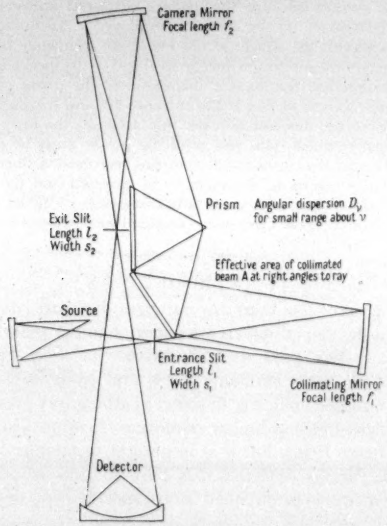


Figure 1. Elementary spectrometer.

spectral range $\nu$ to $\nu+\delta\nu$ passing the entrance slit and accepted into the collimated beam is given by

$$W_\nu = \frac{As_1l_1}{f_1^2}\frac{1}{\pi}\int_\nu^{\nu+\delta\nu} E_\nu\, d\nu, \qquad \ldots\ldots(1)$$

where $A$ is the area of the collimator mirror normal to the ray, and we assume the prism is sufficiently large to take all this radiation, $s_1$, $l_1$, $f_1$ are the width and length of the entrance slit and the focal length of the collimating mirror respectively, and $E_\nu$ has its usual value

$$\frac{2\pi\nu^2}{c^2}\frac{h\nu}{\exp(h\nu/kT)-1}.$$

If it is assumed that the interval $\delta\nu$ is sufficiently small for $E_\nu$ to remain constant, $\int_\nu^{\nu+\delta\nu} E_\nu d\nu \simeq E_\nu \delta\nu$, and the energy passing the entrance slit will be dispersed at the exit slit over an area $D_\nu f_2 \delta\nu (l_1 f_2/f_1)$. In this it is assumed either that $\delta\nu$ is large compared with one slit width, so that the expression holds regardless of aberration and diffraction, or that $\delta\nu$ is comparable with a slit width only when this is sufficiently large for aberration and diffraction to be neglected. Here $D_\nu$ is the angular dispersion, also assumed constant over the range $\nu$ to $\nu+\delta\nu$, and $f_2$ is the focal length of the camera mirror. The power $W'_\nu$ passing the exit slit will then be given by the product of the exit slit area and the power per unit area in the dispersed image at the slit. Making the assumption that $s_2/s_1 = l_2/l_1 = f_2/f_1$,

$$W'_\nu = A s_1^2 l_1 E_\nu / D_\nu f_1^3 \pi. \qquad \ldots\ldots(2)$$

In deriving this expression for $W'_\nu$ no account has been taken of deviations of the source from black-body emissivity, or of energy losses occurring on reflection at mirrors or by passage through windows or through the atmosphere. The effective energy stream available at the detector must therefore be $W'_\nu$ multiplied by some loss factor, $x$.

Let $W_0$ be the minimum energy stream which, falling on the detector, will provide some appropriate minimum signal-to-noise ratio $M_0$ at the display. To obtain the best resolving power the slits will be closed until the energy stream at the detector, $xW'_\nu$, becomes equal to $W_0$, when the minimum entrance slit width $s_0$ will be given by

$$s_0^2 = W_0 \pi D_\nu f_1^3 / x E_\nu A l_1. \qquad \ldots\ldots(3)$$

It will be convenient to express performance in terms of a quantity, $\Gamma$, which is the frequency band in $cm^{-1}$ embraced by one slit width. (Separating power will then be proportional to $1/\Gamma$.) Taking again $s_2/s_1 = f_2/f_1$, it appears that $\Gamma_\nu$ for the frequency range $\nu$ to $\nu+\delta\nu$ may be defined, for slit widths at which aberration and diffraction are negligible, as follows:

$$\Gamma_\nu = s_1/D_\nu f_1. \qquad \ldots\ldots(4)$$

It may be noted at this point that $l_1$ is normally made as large as is consistent with a reasonable level of aberration (Perry 1938) and that under these conditions $l_1$ is approximately proportional to $f_1$; $l_1/f_1 = g$. Then, using equation (4),

$$\Gamma_\nu = \sqrt{(W_0 \pi / x D_\nu A E_\nu g)}. \qquad \ldots\ldots(5)$$

## §3. SIMPLIFIED MODEL OF INFRA-RED DETECTOR

It is convenient to assume a simplified model of an infra-red detector and then to specify its performance by means of three parameters. In this idealized detector the temperature difference produced in the receiver by the radiation signal is analogous to the voltage produced across a circuit consisting of a resistance and a capacity in parallel fed from a high-impedance constant-current generator. The resistance corresponds to the path along which heat is lost by re-radiation and conduction, and the capacity to the thermal capacity of the receiver. The product of the resistance and capacity values gives the time constant. The output voltage, $V$, of such a detector when a step of radiation of height $W$ is applied may be represented by

$$V = \sigma W \{1 - \exp(-t/\tau)\}, \qquad \ldots\ldots(6)$$

where $\sigma$ is a steady state sensitivity (say in microvolts per microwatt), $t$ is time commencing from $t=0$ when the radiation is applied, and $\tau$ is the time constant.

In practice, the thermal constants of a receiver are so distributed that for high modulation frequency components of the incident radiation the thermal wavelength in the receiver may be comparable to or smaller than the receiver dimensions, and some form of delay network treatment must be substituted for the simple resistance–capacity circuit postulated in equation (6). Similarly, the heat sink for the receiver may be imperfect, as in some backed bolometers, giving additional time constants greater than $\tau$ of equation (6). Alternatively, a thermal differentiating circuit may exist, as in the Golay cell (Golay 1947), for which $V$ after an initial rise returns more slowly to zero instead of remaining constant.

Since, for practical purposes, a detector is used with a radiation modulation frequency appropriate to its time constant, it appears reasonable to accept values of $\sigma$ and $\tau$ which make equation (6) most nearly fit the experimental $V/t$ plot for the detector in question.

A further parameter, $\mu$, which is a measure of the total noise arising in the detector, must be introduced. Noise in any detector arises in the first place from random fluctuations in the incident and re-radiated energy streams or in the temperature of the receiver (Daunt 1945, Jones 1947, Lewis 1947, Milatz and van der Velden 1943) and in the second place from electrical fluctuations—Johnson noise, shot noise, current and contact noise of various types. For Johnson noise the mean square fluctuation voltage, $\overline{V}_n^2$ appearing across a resistance $R$ at absolute temperature $T$ for bandwidth $\Delta f$ is given by

$$\overline{V}_n^2 = 4\boldsymbol{k}TR\Delta f, \qquad \ldots\ldots(7)$$

with correspondingly more general relations for networks having reactance (Nyquist 1928, Johnson 1928).

In a receiver system consisting of detector, amplifier and display, it is in general technically possible to make the noise level at the display dependent only on the detector noise properties and on the effective bandwidth of amplifier and display where, as is usual, this is smaller than the detector bandwidth. Thus it appears desirable to express the observed part of the mean square fluctuation voltage at the detector output as

$$\overline{V}_n^2 = \mu\Delta f, \qquad \ldots\ldots(8)$$

where $\mu$ is characteristic of the detector alone and $\Delta f$ is normally characteristic of the amplifier and display alone. It is assumed that $\mu$ covers detector noise of all types mentioned above. It may therefore vary with the frequency at which the pass-band $\Delta f$ occurs, particularly in the case of current and contact noise. Since, however, the more fundamental types of noise have a comparatively uniform frequency spectrum over the detector operating ranges considered, we shall assume, for simplicity, that $\mu$ is constant for any given detector.

## §4. "CHOPPED-BEAM" AND "VIDEO" SYSTEMS OF PRESENTATION

Using the parameters $\sigma$, $\tau$, and $\mu$ as defined above, it is possible to find an expression for $W_0$ for a receiver system including a particular detector. The first system to be considered will be that in which the incident radiation is chopped, the radiation pulses having duration $a$, the effective bandwidth from the point of view of noise, $\Delta f$, being defined as a display bandwidth extending from zero frequency to $1/a$. The peak signal voltage, $V_s$, reached at the detector output when a pulse of radiation of height $W_0$ and duration $a$ is applied is given by

$$V_s = \sigma W_0\{1-\exp(-a/\tau)\}. \qquad \ldots\ldots(9)$$

The detector r.m.s. noise voltage observable by means of the amplifier and display is given by $\overline{V}_n = \sqrt{(\mu \Delta f)} = \sqrt{(\mu/a)}$, corresponding to a peak-to-peak noise voltage, $V_p$, riding on the signal and given by

$$V_p = q\sqrt{(\mu/a)}, \qquad \ldots\ldots(10)$$

where $q$ has a value of 6 to 8 (Rice 1944). Then for a minimum acceptable signal-to-noise ratio, $M_0$, at the display

$$W_0 = \frac{qM_0\sqrt{\mu}}{\sigma\{1-\exp(-a/\tau)\}\sqrt{a}}. \qquad \ldots\ldots(11)$$

A second system may be considered in which the spectrum traverses the exit slit rapidly, with a scanning speed of $\Sigma$ cm$^{-1}$/sec., and the detector output contains modulation corresponding to the energy changes of the spectrum. In a system of this type, in which the signal is analogous to a television video signal, the amplifier response must extend from zero, or from some relatively low scan repetition frequency, up to a value which is just greater than the maximum modulation frequency occurring in the detector output.

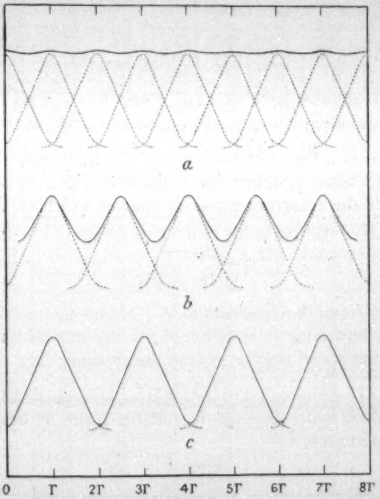


Figure 2. Radiation patterns at spectrometer exit slit on scanning spectra composed of lines at various intervals: (*a*) Γ, (*b*) 3Γ/2, and (*c*) 2Γ.

The connection between maximum modulation frequency of the radiation and scanning speed may be illustrated as follows. Consider a spectrometer (cf. Figure 1) with equal entrance and exit slit widths and with collimating mirror and camera mirror of equal focal lengths, operating under energy limited conditions. For equal inputs of monochromatic radiation at spectral separations of Γ the radiation pattern appearing at the detector as the spectrum is scanned will have the form plotted in Figure 2 (*a*), while for frequency intervals 3Γ/2 and 2Γ the patterns will resemble those plotted in Figures 2 (*b*) and 2 (*c*) respectively. Thus for separating power 1/Γ a signal component of which one cycle corresponds to a wave number range of Γ or greater may be present at the detector. If the scanning speed is Σ,

then the maximum signal frequency at the detector will be $\Sigma/\Gamma$, and this will define the upper limit, $f_m$, of the frequency band to which detector, amplifier and display must respond.

For a component of the radiation signal, $\delta W$, of angular frequency $\omega$, the detector output, $\delta V_s$, will be given by

$$\delta V_s = \frac{\sigma \delta W}{1+\omega^2\tau^2}. \qquad \ldots\ldots(12)$$

If $\omega$ is limited to values less than $1/\tau$, and the amplifier–display response is flat, distortion of the spectrum will not be excessive. If, however, no such limitation is placed on the value of $\omega$, and distortion must not become unmanageable, the response characteristic of the amplifier–display system must be modified. Peak gain must occur for the highest radiation signal frequency component, $f_m$, where $f_m = \Sigma/\Gamma$, and be reduced by the factor $\sqrt{\{(1+\omega^2\tau^2)/(1+\omega_m^2\tau^2)\}}$, where $\omega_m = 2\pi f_m$, for lower values of $\omega$. On this basis the signal voltage, $V_s$, at the display, integrated over the pass-band, will be given by

$$V_s = \sigma W/\sqrt{(1+\omega_m^2\tau^2)}, \qquad \ldots\ldots(13)$$

and the integrated r.m.s. noise voltage by

$$\overline{V}_n = \sqrt{\left\{\left(\frac{\mu f_m}{3}\right)\left(1+\frac{2}{1+\omega_m^2\tau^2}\right)\right\}}, \qquad \ldots\ldots(14)$$

which for $\omega_m\tau \ll 1$ reduces to $\overline{V}_n = \sqrt{(\mu f_m)}$ and for $\omega_m\tau \gg 1$ to $\overline{V}_n = \sqrt{(\mu f_m/3)}$. Thus for a minimum acceptable signal-to-noise ratio, $M_0$, at the display

$$W_0 = qM_0\sqrt{\{\mu f_m(1+\omega_m^2\tau^2/3)\}}/\sigma. \qquad \ldots\ldots(15)$$

In the chopped-beam system some suitable number, $\alpha$, of radiation pulses should occur while the spectrum traverses one slit width or $\Gamma\,\mathrm{cm}^{-1}$. Thus the scanning speed is proportional to the number of pulses per second, $p/a$, and to the frequency range covered, $\Gamma$, per $\alpha$ pulses:

$$\Sigma = \Gamma(p/\alpha a), \qquad \ldots\ldots(16)$$

where $p$ is a mark to (mark + space) ratio.

In the video system using an amplifier of flat response within its pass-band the permissible scanning speed is governed by the relation

$$\Sigma = \Gamma/2\pi\tau, \qquad \ldots\ldots(17)$$

while for an amplifier with response of suitable form, as described above, the corresponding condition is

$$\Sigma = f_m\Gamma. \qquad \ldots\ldots(18)$$

## § 5. INTER-RELATION OF SEPARATING POWER AND SCANNING SPEED

The relations derived above may now be used to discuss the inter-dependence of optimum separation, $\Gamma_0$, and scanning speed, $\Sigma_0$, in spectroscopic systems. Consider first the chopped-beam system.

For the case in which the energy stream entering the spectrometer is strictly limited the relevant equations are (5), (11) and (16). From these it will be seen that $\Gamma$ can be plotted as a function of $a$, the radiation pulse length, as can $\Sigma$. Corresponding values of $\Gamma$ and $\Sigma$ for a given system may then be used to yield a curve which represents complete information on the performance of the system. Curves of this type, based on spectrometer and detector data set out in an appendix to this account, are given in Figure 3.

A typical curve of log Γ against log Σ, as shown in Figure 3, may be considered to be made up of four distinct sections with fairly well marked inflections between

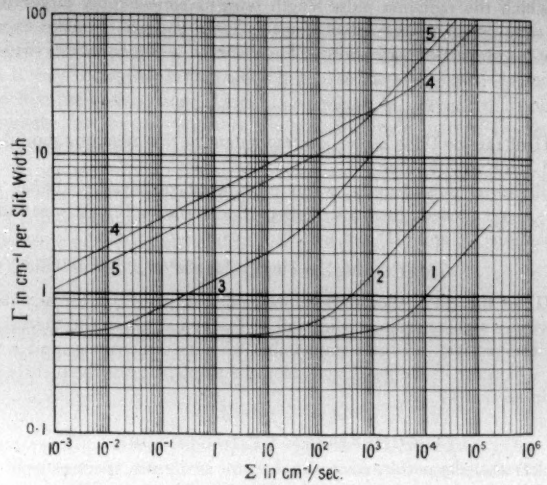


Figure 3. Plot of log Γ against log Σ for (1) photoconductive cell, (2) superconducting bolometer, (3) Schwarz type thermopile, (4) Golay cell and (5) thermistor bolometer.

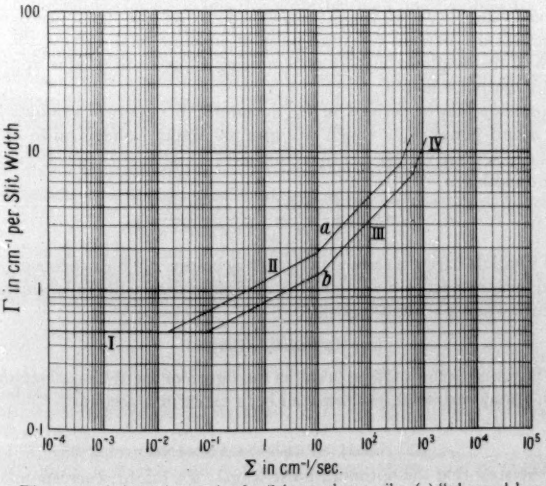


Figure 4. Diagrammatic log Γ/log Σ plot for Schwarz thermopile: (*a*) "chopped beam" system, (*b*) "video" system.

them (cf. Figure 4 (*a*)). For very low values of scanning speed the resolving power is limited by optical aberration and diffraction and tends to become approximately

constant, corresponding to section I of the $\log \Gamma/\log \Sigma$ curve at the left of Figure 4. At higher values of scanning speed, for which the system becomes energy-limited but for which the radiation pulse length remains considerably larger then the detector time constant, the value of $a/\tau$ is large enough to make $\exp(-a/\tau)$ negligible in comparison with unity. For this case using equations (5) and (11) and writing $1-\exp(-a/\tau) \simeq 1$ and $\xi = \pi q M_0 \sqrt{\mu/x} D_v A E_v g \sigma$,

$$5 \log \Gamma - \log \Sigma = 2 \log \xi + \log \alpha/p. \qquad \ldots\ldots(19)$$

Section II of the $\log \Gamma/\log \Sigma$ plot, corresponding to this relation, should have a slope of 1/5 for any detector.

At still shorter pulse lengths, where $a$ becomes considerably shorter than $\tau$, $1-\exp(-a/\tau) \simeq a/\tau$ and a further straight portion of the $\log \Gamma/\log \Sigma$ plot will occur. Using equations (5) and (11) and writing $1-\exp(-a/\tau) = a/\tau$,

$$7 \log \Gamma - 3 \log \Sigma = 2 \log \xi + \log \tau^2 \alpha^3/p^3. \qquad \ldots\ldots(20)$$

Section III of the curve should therefore have a slope of 3/7 for any detector. As $a/\tau$ becomes smaller again, a point will be reached at which the thermal wavelength in the receiver becomes comparable with its dimensions, and a further inflection will occur in the $\log \Gamma/\log \Sigma$ plot, the slope being subsequently greater than 3/7 in section IV.

## §6. COMPARISON OF DETECTORS

It is clear that the performance of a detector in a given spectroscopic system may be fairly completely represented by a $\log \Gamma/\log \Sigma$ curve. One may enquire, however, if there is any way of expressing detector performance by means of a single figure of merit. Such a criterion may be found if the assumption is made that the most valuable detector is one which will give a pulse signal just detectable above noise for an incident radiation pulse of smallest total energy, the overall bandwidth of the amplifier–display system being adjusted to a value appropriate to the radiation pulse length.

An expression may be derived for $U_0$, the minimum energy of a radiation pulse of length $a$ and power $U_0/a$ which will give an output voltage pulse of height $qM_0$ times r.m.s. noise voltage. From equation (11), setting $U_0/a = W_0$ and again taking bandwidth $1/a$,

$$U_0 = qM_0 \left[\frac{\sqrt{(\mu\tau)}}{\sigma}\right] \frac{\sqrt{(a/\tau)}}{1-\exp(-a/\tau)}, \qquad \ldots\ldots(21)$$

where the symbols have the same significance as before. This expression may be minimized with respect to $a/\tau$ to give the minimum detectable pulse energy, $U_0$, which occurs when $a = 1{\cdot}256\tau$, giving

$$U_0 = 1{\cdot}567 qM_0 \sqrt{(\mu\tau)}/\sigma. \qquad \ldots\ldots(22)$$

Thus the factor $\sqrt{(\mu\tau)}/\sigma$ may be taken as the figure of merit of a detector when sensitivity, speed and noise level have all been taken into account.

## §7. HIGH SPEED SCANNING

It will be seen that the optimum pulse length, $a = 1{\cdot}256\tau$, corresponds to the inflection between section II and section III of the $\log \Gamma/\log \Sigma$ plot of Figure 4, and that at this point

$$W_0 \simeq 1{\cdot}25 (qM_0/\sigma) \sqrt{(\mu/\tau)}. \qquad \ldots\ldots(23)$$

If the infra-red source brightness is unrestricted, and no limits are placed on $\Gamma$ or $\Sigma$, it appears that equation (23), together with equation (5) and equation (16), specify the best operating conditions.

It is clear that a detector may be operated at radiation chopping frequencies higher than this optimum if a sufficiently high value of $W_0$ is attainable, and in practice it may be profitable to operate the detector at chopping frequencies up to the inflection between sections III and IV of Figure 4. Beyond this point, in the region where for thermo-detectors the standing-wave pattern in the receiver (and for photo-detectors the duration of the primary photoelectric process) become important, a rapid falling off in detector performance may be expected.

If the video system of presentation is now considered it is seen that again the $\log \Gamma / \log \Sigma$ plot falls into four distinct sections, as shown in Figure 4 (*b*), the first being determined by purely optical considerations. From equations (5), (15) and (18), for the region in which $\omega_m^2 \tau^2 \ll 1$,

$$5 \log \Gamma - \log \Sigma = 2 \log \xi, \qquad \ldots\ldots (24)$$

and the curve has a slope of 1/5, as in section II of Figure 4 (*b*).

If a flat amplifier response is used, section III of the $\log \Gamma / \log \Sigma$ plot will be determined, in the region where $\omega_m^2 \tau^2 \gg 1$, by equation (17). Thus

$$\log \Gamma - \log \Sigma = \log 2\pi\tau, \qquad \ldots\ldots (25)$$

giving a slope of 1. For the appropriate amplifier–display response characteristic, if it could be realized, the curve would be determined by equations (5), (15) and (18). These give

$$7 \log \Gamma - 3 \log \Sigma = 2 \log \xi + \log 4\pi^2 \tau^2 / 3, \qquad \ldots\ldots (26)$$

for which the slope is 3/7. Thus it is seen that $\log \Gamma / \log \Sigma$ curves for the video system run parallel, in sections II and III to the corresponding curves for the chopped-beam system, but lie below them, indicating that the video method of presentation, if it should prove technically feasible, would use any given detector more efficiently than the chopped-beam method. With the exception of standard D.C. amplification systems, which may be considered as a special case of video presentation, the possibility of constructing amplifiers of suitable phase and amplitude response characteristics has not been fully investigated.

ACKNOWLEDGMENT

One of us (E.F.D) is indebted to the Institute of Petroleum for a maintenance grant, during the tenure of which the work was initiated. It was completed during his tenure of an Imperial Chemical Industries Fellowship.

REFERENCES

Andrews, D. H., Milton, R. M., and de Sorbo, W., 1946, *J. Opt. Soc. Amer.*, **36**, 353, and **36**, 518.

Barnes, R. B., McDonald, R. S., Williams, V. Z., and Kinnaird, R. F., 1945, *J. Appl. Phys.*, **16**, 77.

Becker, J. A., and Moore, H. R., 1946, *J. Opt. Soc. Amer.*, **36**, 354.

Bell, E. E., Buhl, R. F., Nielsen, A. H., and Nielsen, H. H., 1946, *J. Opt. Soc. Amer.*, **36**, 355.

Bell Telephone Laboratories, 1946, Information supplied by Bell Telephone Laboratories.

Daly, E. F., and Sutherland, G. B. B. M., 1947, *Proc. Phys. Soc.*, **59**, 77.

DAUNT, J. G., 1945, Unpublished report circulated by Admiralty.
EPPLEY LABORATORIES, 1947, Information supplied by Eppley Laboratories.
GOLAY, M. J. E., 1947, *Rev. Sci. Instrun.*, **18,** 347, and **18,** 357.
HILGER, ADAM, 1947, Information supplied by Messrs. Adam Hilger Ltd.
JOHNSON, J. B., 1928, *Phys. Rev.*, **32,** 97.
JONES, R. C., 1947, *J. Opt. Soc. Amer.*, **37,** 879.
LEWIS, W. G., 1947, *Proc. Phys. Soc.*, **59,** 34.
MILATZ, J. M. W., and VAN DER VELDEN, H. A., 1943, *Physica*, **10,** 369.
MILTON, R. M., 1946, *Chem. Rev.*, **39,** 403.
NYQUIST, H., 1928, *Phys. Rev.*, **32,** 110.
OXLEY, C. L., 1946, *J. Opt. Soc. Amer.*, **36,** 356.
PERKIN ELMER CORPN., 1947, Information supplied by Perkin Elmer Corporation.
PERRY, J. W., 1938, *Proc. Phys. Soc.*, **50,** 265.
RICE, S. O., 1944, *Bell System Tech. J.*, **23,** 282, also 1945, **24,** 46.
SIMPSON, O., SUTHERLAND, G. B. B. M., and BLACKWELL, D. E., 1948, *Nature, Lond.*, **161,** 281.
SUTHERLAND, G. B. B. M., BLACKWELL, D. E., and FELLGETT, P. B., 1946, *Nature, Lond.*, **158,** 875.
SUTHERLAND, G. B. B. M., and LEE, E., 1948, *Reports on Progress in Physics*, Vol. XI (London : Physical Society), p. 144.
WEISS, R. A., 1946, *J. Opt. Soc. Amer.*, **36,** 356.
WILLIAMS, V. Z., 1948, *Rev. Sci. Instrun.*, **19,** 135.

## APPENDIX

In computing the $\log \Gamma / \log \Sigma$ plots given in Figures 3 and 4 the optical system assumed is that of the Perkin Elmer Corporation Model 12 B spectrometer (Barnes *et al.* 1945) using a lithium fluoride prism at 2,000 $cm^{-1}$.

| | | |
|---|---|---|
| $D$ | Angular dispersion at 2,000 $cm^{-1}$ | $8{\cdot}7 \times 10^{-5}$ radian/$cm^{-1}$ |
| $A$ | Effective prism area | 30 $cm^2$ |
| $E$ | Black-body radiation, 2,000 $cm^{-1}$ | $3 \times 10^{-3}$ watt/$cm^{-1}$/$cm^2$ |
| $l_1$ | Slit length ($l_1 = l_2$) | 1·2 cm. |
| $f_1$ | Collimator mirror focal length | 27 cm. |
| $x$ | Loss factor | 0·25 |
| $M_0$ | Min. S/N required at display | 50 |
| $q$ | Peak-to-peak to r.m.s. ratio | 8 |
| $k$ | Boltzmann's constant | $1{\cdot}37 \times 10^{-23}$ joules/deg. |
| $p$ | Mark to mark + space ratio | 0·5 |
| $a$ | Number of pulses per slit width | 3 |

In obtaining data on the parameters $\sigma$, $\tau$, and $\mu$ for various detectors the Table given below was compiled. It was found that information on $\mu$ and $\sigma$ separately was in most cases not available. Where a value of the energy stream, $W_{M=1}$, for which the signal voltage equals r.m.s. noise voltage, could be found, $\sqrt{\mu}/\sigma$ was obtained from this using the relation $\sqrt{\mu}/\sigma = W_{M=1}/\Delta f$ where $\Delta f$ is the noise bandwidth.

The quantity $\sqrt{(\mu\tau)}/\sigma$ is useful as a basis for comparing detectors, and detector performances given in the table are arranged in approximate order of merit in this way. The minimum detectable pulse energy, $U_0$, may be obtained by multiplying the value of $\sqrt{(\mu\tau)}/\sigma$ by the factor $1{\cdot}567 q M_0$ which, for a pulse just distinguishable above noise, might have a value of 10. From the Table probable values of $\tau$ and $\sqrt{\mu}/\sigma$ for the five types of detector considered were obtained and are used in computing the curves of Figures 3 and 4. It may be noted that the value for photoconductive cells is for peak spectral sensitivity, and hence is not strictly applicable when the basis of computation is a spectrometer set at 2,000 $cm^{-1}$.

Values of the constants occurring in equations (19), (20), (24) and (26) are as follows :

$$\log \xi = 10{\cdot}7014 + \log \sqrt{\mu}/\sigma, \qquad \log \tau^2\alpha^3/p^3 = 2{\cdot}3343 + 2\log\tau,$$
$$\log \alpha/p = 0{\cdot}7781, \qquad \log 4\pi^2\tau^2/3 = 1{\cdot}1191 + 2\log\tau.$$

Values assumed in computing Figure 3 are as follows:

| Detector | Curve (Fig. 3) | $\tau$ | $\sqrt{\mu}/\sigma$ |
|---|---|---|---|
| Photoconductive cell | 1 | $2\times10^{-4}$ | $2\times10^{-14}$ |
| Superconducting bolometer | 2 | $5\times10^{-4}$ | $10^{-12}$ |
| Schwarz type thermopile | 3 | $10^{-2}$ | $5\times10^{-11}$ |
| Golay cell | 4 | $5\times10^{-4}$ | $2\times10^{-9}$ |
| Thermistor bolometer | 5 | $5\times10^{-3}$ | $10^{-9}$ |

In computing Figure 4, which is purely diagrammatic, constants for a particular Schwarz thermopile were used, and the effect of distributed thermal capacity in the receiver taken to be of importance at signal frequencies above 100 c/s. In this case $\tau = 4\times10^{-2}$ and $\sqrt{\mu}/\sigma = 4\times10^{-11}$.

| Detector | $\tau$ (sec.) | $\frac{\sqrt{\mu}}{\sigma}$ | $\frac{\sqrt{(\mu\tau)}}{\sigma}$ | Area ($cm^2$) | Res. (ohm) | References and Notes |
|---|---|---|---|---|---|---|
| Photo-conductive cells. | $1{\cdot}5\times10^{-4}$ | $1{\cdot}7\times10^{-14}$ | $2{\cdot}1\times10^{-16}$ | 0·01 | $7{\cdot}5\times10^{6}$ | Simpson *et al.* 1948, PbTe cell, 2·2 $\mu$ peak at 83° K. |
| | $10^{-4}$ | $3{\cdot}7\times10^{-13}$ | $3{\cdot}7\times10^{-15}$ | — | $3\times10^{6}$ | Sutherland *et al.* 1946 PbS cell, 2·5 $\mu$ peak, 200° K. |
| | $10^{-4}$ | $2{\cdot}8\times10^{-12}$ | $2{\cdot}8\times10^{-14}$ | 0·09 | — | Oxley 1946, German chemical PbS cell |
| Super-conducting bolometers | $5\times10^{-4}$ | $8{\cdot}9\times10^{-13}$ | $2\times10^{-14}$ | 0·01 | 5 | Andrews *et al.* 1946 |
| | $1{\cdot}8\times10^{-4}$ | $1{\cdot}8\times10^{-12}$ | $2{\cdot}4\times10^{-14}$ | 0·008 | 1·6 | Milton 1946 |
| | $1{\cdot}8\times10^{-3}$ | $1{\cdot}2\times10^{-11}$ | $5\times10^{-13}$ | 0·008 | 0·3 | Bell *et al.* 1946 |
| Schwarz type thermopiles | $8\times10^{-3}$ | $5{\cdot}7\times10^{-11}$ | $5{\cdot}1\times10^{-12}$ | 0·004 | 20 | Perkin Elmer 1947 |
| | $3{\cdot}6\times10^{-2}$ | $3{\cdot}3\times10^{-11}$ | $6{\cdot}3\times10^{-12}$ | 0·004 | 60 | Hilger 1947 |
| Golay cells | $3{\cdot}4\times10^{-4}$ | $1{\cdot}6\times10^{-9}$ | $2{\cdot}9\times10^{-11}$ | — | — | Weiss 1946 |
| | $5\times10^{-3}$ | $7{\cdot}1\times10^{-9}$ | $5\times10^{-10}$ | 0·025 | — | Eppley 1947 |
| Thermistor bolometers | $5\times10^{-3}$ | $7{\cdot}3\times10^{-10}$ | $5{\cdot}1\times10^{-11}$ | 0·006 | $2\times10^{6}$ | Becker & Moore 1946 |
| | $9\times10^{-3}$ | $1{\cdot}3\times10^{-9}$ | $1{\cdot}2\times10^{-10}$ | 0·004 | $2\times10^{6}$ | Bell Tel. Labs. 1947 |

# The Luminescence of Wetted Solids

By J. EWLES and G. C. FARNELL*
Department of Physics, The University of Leeds

*MS. received* 25*th July* 1948, *in amended form* 25*th November* 1948

*ABSTRACT.* An earlier observation that the association of a non-luminescent pure liquid with a non-luminescent solid produces fluorescence and phosphorescence in the liquid has been confirmed. The luminescent spectra of water, heavy water, and alcohols, as well as some other liquids with different negative radicals when adsorbed by various finely divided ionic solids have been examined and recorded. The positions of the maxima of the main broad band are very similar for all the hydroxy liquids even with different solids (band peaks in the range 4300–4500 A.) and are different for the same solid with liquids having different negative radicals. Preliminary experiments on the relation between brightness and relative amount of liquid indicate that the phenomena are associated with the active sites on the solid surface, and afford evidence of the existence of these and of their differences on the same solid.

Excitation spectra confirm preliminary observations that the adsorbed molecules have very abnormal absorption regions indicating considerable changes in energy levels. Two suggestions are made to explain the phenomena: (*a*) the energy changes may be correlated with the heat of adsorption on the active sites; (*b*) the adsorbed molecules are bonded to the solid by the positive radicals leaving an almost free negative ion.

## §1. INTRODUCTION

It was observed earlier (Ewles 1930, Ewles and Martin 1939) that many white solids when wetted with water showed, on excitation by the near ultra-violet, a faint blue fluorescence and a phosphorescence lasting for some seconds. On complete drying of the solid the luminescence disappeared. Later observations showed that the spectral distribution of the luminescence was astonishingly similar for different solids. The implication of this effect—that the mere contact of liquid with solid, both separately transparent into the far ultra-violet and both non-luminescent, is sufficient to endow the system with the power of luminescence under excitation by wavelengths which are not normally absorbed—clearly required confirmation.

## §2. CONFIRMATION OF THE REALITY OF THE PHENOMENON

(*a*) *The glow might be due to modified scattering.*

In such a case the spectrum would be dependent on the spectral distribution of the exciting light. This was found not to be so. Further, the existence of phosphorescence having the same spectral distribution as the fluorescence makes the scattering hypothesis extremely unlikely since there is so far no evidence for any time lag in the emission of scattered radiation.

(*b*) *The solid itself might be luminescent, even when dry.*

The earlier investigations referred to above were extended and confirmed. Wetted silica and wetted sodium chloride showing quite a marked blue glow were dried by continued heating *in vacuo*. After three to four hours at 500° C. for silica and half an hour for sodium chloride all traces of the blue glow had

* Now at the Kodak Research Laboratories, Wealdstone, Middx.

disappeared, even under the strongest excitation with light of wavelengths down to 3000 A. and with the specimen at a temperature of 90° K. Rewetting *in vacuo* restored in large measure the power of glowing under and after excitation.

(*c*) *The pure liquid might be luminescent.*

Tap water was found to possess a marked luminescence, especially at 90° K. Doubly distilled water, however, showed no trace of glow under the same conditions.

(*d*) *A soluble impurity in the solid might give a luminescent solution on wetting.*

To test this the silica powder was boiled with doubly distilled water in a carefully cleaned silica flask for some hours. The water remaining was decanted and set aside. Fresh doubly distilled water was added to the silica and the process repeated. After many repetitions the wetted silica in the flask was found to retain undiminished its power of glowing, while none of the decanted samples of water showed any trace of luminescence.

Thus it seems fairly certain that the blue glow is not due to the formation of a luminescent solution on wetting the solid.

(*e*) *The luminescence might be caused by gases dissolved in the water and adsorbed by the solid on wetting.*

This possibility appears to be eliminated by the facts that (i) rewetting *in vacuo* of the silica dried *in vacuo* by water which has been doubly distilled and then boiled for several minutes produces the same effect as rewetting in air; (ii) after removal of the luminescence by drying *in vacuo* the readmission of dry air causes no restoration of the luminescence even on long standing.

These experiments thus appear to confirm the previous observations and conclusions that the mere contact of a suitable liquid with a white solid confers on the associated system the power of fluorescence and phosphorescence under excitation by light not normally absorbed by either separately.

## § 3. INVESTIGATIONS OF THE LUMINESCENT SPECTRA OF WETTED SOLIDS

A Hilger medium quartz spectrograph was mainly employed, with occasional recourse to the Hilger Constant Deviation glass instrument, and to the larger Hilger instrument (f = 170 cm.). For examination of the spectra excited by the near ultra-violet the excitation was from a Mazda 125 watt Mercra lamp with the outer glass envelope removed. The most satisfactory arrangement of complementary filters available for near ultra-violet excitation was a piece of Wood's glass, 6 mm. thick, on the exciting side and a silica cell containing carbon disulphide, of 2·5 cm. thickness, on the spectrograph side. The latter has a very sharp cut-off at 3750 A. and negligible absorption above this wavelength. For the far ultra-violet the very useful Bowen filter (Bowen 1935), consisting of a solution of 145 gm. hydrated nickel sulphate and 41·5 gm. hydrated cobalt sulphate in 1,000 ml. of water, was employed (a 10 cm. thickness of this filter was used, in a "stopped-down" silica flask of 10 cm. diameter). This filter has a useful transmission below about 3300 A. while cutting off between that region and the yellow.

For examination of the fluorescence and phosphorescence at low temperatures the specimens were mounted as shown in Figures 1 and 2.

A cardboard cylinder mounted on a wooden disc attached to the vertical spindle of an electric motor is provided with two horizontal slots JJ of angular aperture just less than the angular distance between the windows W. This

means that when the specimen is just seen by the slit of the spectrograph it is just not illuminated by the exciting light. For fluorescence work an extra aperture is provided in the cardboard cylinder which can be opened or covered as desired. The speed of rotation of the cardboard cylinder (usually a few revolutions a second) could be controlled to give visually the brightest phosphorescence for the sample being investigated. The solids were prepared in the form of very fine powders from A.R. standard substances and were purified by repeated

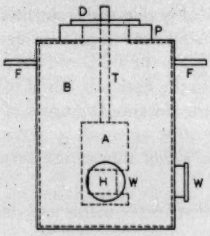


Figure 1. The low temperature specimen mounting. B—vacuum tight brass cylindrical box; FF—side tubes; P—Pyrex annulus; A—brass cylindrical box; H—hemicylindrical gap with flat vertical back for mounting of specimen; T—invar tube; D—brass disc; W—quartz windows.

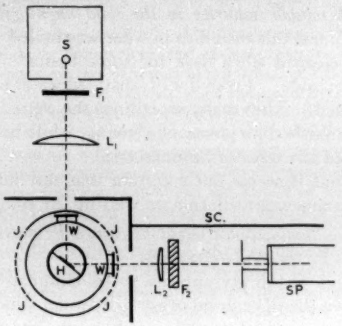


Figure 2. Horizontal section of the general arrangement of apparatus for the recording of emission spectra. S—light source; $F_1F_2$—complementary filters; $L_1L_2$—quartz focusing lenses; JJ—slots in rotating phosphoroscope cylinder; SP—spectrograph collimator; SC—screening.

re-crystallization or precipitation, except in the case of the silica which had been precipitated from ethyl silicate and needed no further purification except repeated washing with doubly distilled water. Where liquids other than water were employed for activation the solids were freed from water by drying *in vacuo* and rewetted *in vacuo* with the pure, redistilled liquid. In every case the absence of luminescence of the dried solids was checked.

The spectrograms, for the most part, were recorded on Ilford H.P.3. plates and photometered with a Cambridge recording photoelectric photometer, the photometer curves being corrected by the aid of a wavelength–sensitivity graph kindly supplied to us by Messrs. Ilford Limited.

The results are summarized in Tables 1, 2 and 3, and some examples of the photometer curves of the spectra are shown in Figures 3, 4 and 7. In the case of solids wetted with water or alcohols the spectra consist mainly of a broad unresolved band stretching from the blue-green to the violet. In some cases there were indications of weak and ill defined bands with peaks at about 5200 A. and 5900 A., but these are doubtful and only the position of the main peak is given in Tables 1 and 2. Attempts to obtain resolution at 90° K. with the large Hilger spectrograph (f = 170 cm.) were unsuccessful.

The features of the spectra to which we now draw attention are:—

(*a*) A similarity between different solids wetted by water but a difference in the peak values of the main band which exceed, sometimes considerably, the probable error (20 A.). (See Table 1)

(*b*) The shift of about 4000 A. to the high frequency side on replacing ordinary water by heavy water. (The heavy water was supplied by I.C.I., Ltd., and was given as 99·77% pure.)

(*c*) The similarity between the spectra of the same solid wetted by different hydroxy liquids but with significant differences, exceeding the experimental tolerance, in the main peak values with different positive radicals, e.g. $SiO_2$–$H_2O$ 4367 A., $SiO_2$–$D_2O$ 3911 A., $SiO_2$–$CH_3OH$ 4266 A., $SiO_2$–$C_2H_5OH$ 4353 A. (low temperature fluorescence).

(*d*) The agreement, within the experimental tolerance, of the peak values for fluorescence and phosphorescence.

(*e*) A shift of the main peak to shorter wavelengths at lower temperatures.

Table 1. Main Band Peaks of Luminescence of Water Wetted Solids

| Solid | (1) (A.) | (2) (A.) | (3) (A.) | Solid | (1) (A.) | (2) (A.) | (3) (A.) |
|---|---|---|---|---|---|---|---|
| $SiO_2$ | 4405 | 4367 | 4360 | KCl | — | 4369 | — |
| $SiO_2(D_2O)$ | 3968 | 3911 | — | BeO | 4316 | — | — |
| $CaF_2$ | 4578 | 4540 | — | $Al_2O_3$ | 4505 | 4488 | — |
| LiF | 4411 | 4390 | — | $CaCO_3$ | — | — | 4444 |
| NaF | 4426 | 4392 | — | $HgCl_2$ | — | — | 4359 |
| NaCl | — | 4431 | 4420 | | | | |

(1) Fluorescent emission. Ordinary temperatures.
(2) Fluorescent emission. Low temperatures.
(3) Phosphorescent emission. Low temperatures.

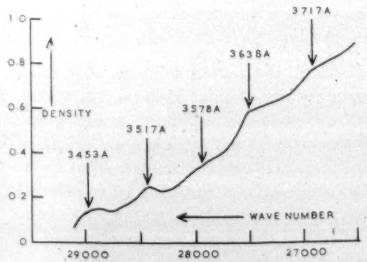


Figure 3. Ultra-violet section of photometer record of fluorescence spectrogram of silica wetted with propylene dichloride (specimen at 90° K.).

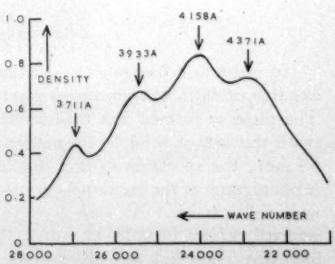


Figure 4. Violet and ultra-violet section of photometer record of fluorescence spectrogram of silica wetted with ethyl bromide (specimen at 90° K.).

Table 2. Main Band Peaks of Luminescence of Solids Wetted by Alcohols

| System | (1) (A.) | (2) (A.) | (3) (A.) | System | (1) (A.) | (2) (A.) | (3) (A.) |
|---|---|---|---|---|---|---|---|
| $SiO_2(CH_3OH)$ | 4289 | 4266 | — | $NaCl(CH_3OH)$ | — | — | 4464 |
| $SiO_2(C_2H_5OH)$ | 4402 | 4357 | — | $NaCl(C_2H_5OH)$ | — | — | 4490 |
| $KCl(C_2H_5OH)$ | 4353 | 4305 | 4311 | | | | |

(1) Fluorescent emission. Ordinary temperatures.
(2) Fluorescent emission. Low temperatures.
(3) Phosphorescent emission. Low temperatures.

Table 3. Luminescence of Silica Wetted by Non-hydroxy Liquids

| System | Luminescent Emission | Details of Fluorescent Spectra |
|---|---|---|
| $SiO_2(C_2H_4Cl_2)$ | Bluish-violet fluorescence and blue phosphorescence under near and far u-v. excitation. | At 90° K. single broad band with peak at 4274 A. |
| $SiO_2(CH_3 . CHCl . CH_2Cl)$ | Bluish white fluorescence and green phosphorescence under near and far u-v. excitation. | At ordinary temperatures a single broad band with peak at 3984 A. At 90° K. broad band, peak at 4148 A. with series of narrow bands on u-v. flank at 3453 A., 3517 A., 3578 A., 3638 A., 3717 A. (See Plate I, and photometer curve, Figure 3.) |
| $SiO_2(C_2H_5Br)$ | Bluish green fluorescence and green phosphorescence under both near and far u-v. excitation. | At 90° K. four well defined peaks in emission band at 4371 A., 4158 A., 3933 A. and 3711 A. (See photometer curve, Figure 4.) |
| $SiO_2(C_2H_5I)$ | Bluish white fluorescence and bluish-green phosphorescence under near u-v. excitation. No emission under far u-v. excitation. | At 90° K. a single broad band with peak at 4320 A. |

## §4. EXCITATION SPECTRA

In order to investigate the excitation spectra the wetted solid was deposited as a thin uniform layer on a glass plate fitting the plate holder of the spectrograph. The plate so formed was then placed in the plate holder of the spectrograph (with the wetted solid layer facing into the camera) and, using a slit width of 0·5 mm., the spectrum of the source was projected on the wetted solid layer. A photograph of the excitation spectrum so produced was recorded by an external wide field camera. An Ilford "Q" filter was placed in front of the lens of the external camera in order to reduce the effects of the short wavelength exciting light that might leak through the powder layer and plate.

An intense source giving a continuous spectrum of adequate intensity and uniformity over the complete exciting wavelength region was not available. In the end we were forced to employ the discontinuous spectrum of the high pressure mercury vapour lamp and an approximate evaluation of the excitation spectrum was made in the following way. The excitation spectrum, having been excited and photographed as indicated above, was photometered and the densities of the lines appearing thereon compared with the densities of the corresponding mercury lines in the direct spectrum recorded on the same kind of plate and with the same slit width (0·5 mm.). The results for the silica–water system are shown in Figure 5 and examples of the excitation spectra in Plate II.

We are not certain as to the reality of the broad excitation band with peak at about 3650 A. since the filters were by no means perfect and the emission of the high pressure Hg arc is very strong in this region. The curve indicates with

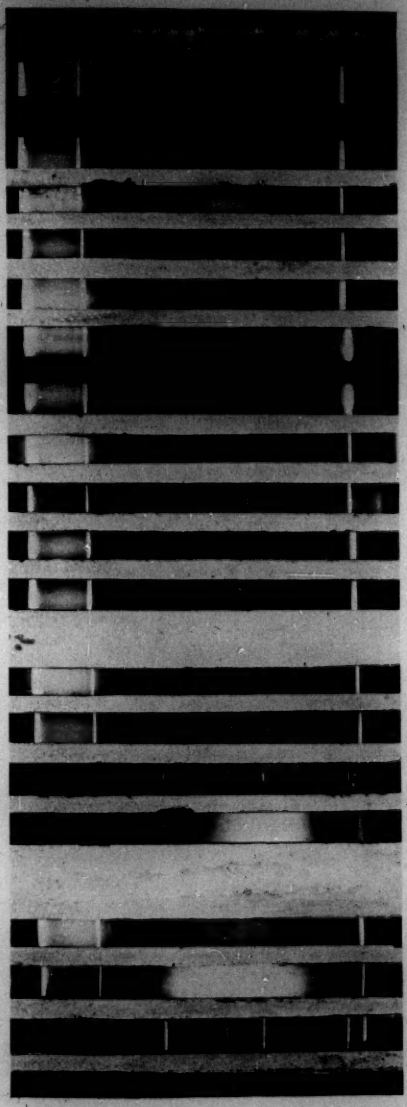
Filter paper { Room Temp. −180°c.
$SiO_2 . H_2O$ Room Temp.
$SiO_2 . D_2O$ Room Temp.
$SiO_2 . D_2O$ −180°c.
NaCl. $H_2O$ −180°c.
NaCl . $H_2O$ Room Temp.
$CaF_2 . H_2O$ Room Temp.
$CaF_2 . H_2O$ −180°c.
LiF . $H_2O$ Room Temp.
LiF . $H_2O$ −180°c.
$SiO_2 . CH_3OH$ −180°c.
$SiO_2 . C_2H_5OH$ −180°c.
NaCl. $CH_3OH$ −180°c.
NaCl . $C_2H_5OH$ −180°c.
$SiO_2 . C_2H_5Br$ −180°c.
$SiO_2 . CH_2CHCl.CH_2Cl$ −180°c.
Hg
$SiO_2 . C_2H_5I$ −180°c.

Plate I.

*To face page 220*

Plate II.

Excitation spectra with Hg vapour lamp.

some certainty, however, the start of excitation at about 4000 A., in agreement with the preliminary observations with selective filters referred to above, and indicates a definite strong peak at about 3130 A. Very similar results were obtained with lithium fluoride wetted with water.

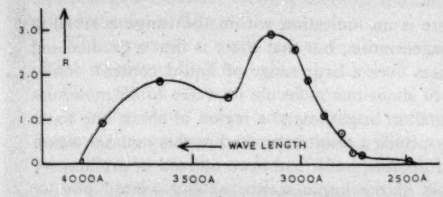


Figure 5. Qualitative representation of excitation spectrum of silica wetted with water.

$$R = \frac{\text{Density of line in excitation spectrum}}{\text{Density of line in direct mercury spectrum}}$$

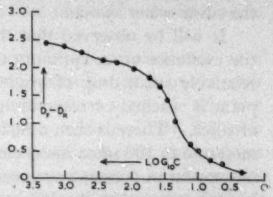


Figure 6. Variation of luminescence brightness with water content of wetted silica.
$D_F - D_R$ = net photographic density produced by image of fluorescent specimen.
$C$ = water concentration in molecules $H_2O : SiO_2 \times 10^3$.

Thus it seems certain that water adsorbed by silica or lithium fluoride is able to absorb radiation of wavelengths not absorbed by the liquid in bulk and, as indicated by the phosphorescence, to possess metastable levels not normally present.

## §5. RELATION BETWEEN BRIGHTNESS OF LUMINESCENCE AND LIQUID–SOLID RATIO

The exciting light from a high pressure mercury lamp, after filtering through 6 mm. of Wood's glass, was focused on a thoroughly wetted specimen contained as a thin layer in a circular graphite capsule, 21 mm. in diameter, and 3 mm. deep, with thin walls and bottom. The graphite forms a container which is black and non-luminescent, light in weight, relatively inert chemically and relatively non-hygroscopic. A film camera of aperture f/2·9 was set at such a distance from the glowing specimen as to give an image of 2 mm. diameter. A Wratten filter having a reasonable transmission for the peak of the main luminescent band and a carbon bisulphide cell, 2·5 cm. thick, were found to form a fairly efficient complementary filter combination to the Wood's glass. The graphite cell with its specimen of wetted solid was removed for weighing immediately after each photograph and then some liquid removed from the specimen by placing the cell in a glass tube connected to a vacuum pump. For the latter stages of water removal gentle heating was also applied. The cell was replaced in exactly the same position after each weighing and water removal, the camera film moved on 1 cm. and a new photograph of the glowing specimen taken. This procedure was repeated until no further loss of weight could be obtained, even after prolonged heating *in vacuo*. The image spots were photometered on the Cambridge photometer referred to previously. The evaluation of relative brightness cannot of course be carried out from these density measurements alone even if the Schwarzschild law of blackening is assumed to hold strictly.

But putting $D_F$ = density of image of fluorescent spot, $D_R$ = density of residual spot due to slight transmission of the exciting radiation by the filter system (i.e. density of spot when fluorescence brightness is reduced to zero, in practice about 0·2), and plotting $D_F - D_R$ against the liquid–solid ratio, a curve results which appears to possess some interest. Such a plot is shown in Figure 6 for the silica–water system.

It will be observed that there is no indication within the range covered of the existence of an optimum concentration, but that there is first a gradual and relatively small drop of brightness over a large range of liquid content until a point is reached corresponding to about one molecule of water to 25 molecules of silica. There is then a rapid fall in brightness to a region of about one water molecule to 100 silica molecules. Such a result expressed in this manner would not appear to possess any special interest, but it had been noticed in preliminary investigations that the brightness of the luminescence of any wetted powder was clearly connected with the size of the particles; the smaller these were the brighter the luminescence. These observations, taken in conjunction with the spectral indications that the luminescence is related to adsorption, suggested an attempt to correlate the brightness with the specific surface of the solid (surface area per gm.).

The specific surface of the precipitated silica employed in the brightness–concentration experiments was kindly determined for us by Dr. Ashley and Mr. Catchpole of the Fuel and Metallurgy Department of the University of Leeds. They employed the low temperature nitrogen adsorption method of Brunauer, Emmett and Teller (1938). The value of the specific surface so obtained was 172 $m^2$. Using this value together with the value of 11 $A^2$ for the area of the water molecule (the mean of two values quoted by Brunauer (1944)) it appears that the beginning of the rapid rate of fall of luminescence corresponds to the occupation of about one quarter of the surface by the water molecules. At the moment, we do not wish to assign any particular significance to the actual numbers, for neither the reliability of the underlying assumptions of the Brunauer, Emmett and Teller method nor the accuracy of the brightness determinations warrant this. It does appear reasonably probable, however, that the order is correct, for the size of the particles determined from an x-ray diffraction pattern obtained for us by Dr. G. W. Brindley of the Department of Physics of this University is of the same order as that indicated by the adsorption values. Moreover repetitions of the brightness–concentration curves gave the sudden drop of brightness at about the same point. (Some preliminary results for silica wetted with ethyl alcohol indicate that in this case the onset of the fall in brightness occurs at a coverage corresponding to approximately a monomolecular layer).

## §6. GENERAL SURVEY AND DISCUSSION OF RESULTS

Shifts in the spectral absorption of molecules adsorbed by solids have been observed by de Boer and his collaborators (de Boer 1935), but the production of luminescence by the contact of a non-luminescent liquid, such as pure water, with a non-luminescent solid, such as silica, under excitation by radiation not normally absorbed by either, provides evidence from a new angle that the process of adsorption involves energy changes in the adsorbed molecule. The occurrence of phosphorescence visible for some seconds after excitation indicates the introduction of metastable levels not previously existent, or of some measurable probabilities for normally forbidden transitions. The similarity between the

luminescent spectra of the same solid wetted by hydroxy molecules having different positive radicals, and the marked difference introduced by substituting heavy water for ordinary water, or in replacing the $-OH$ radical by another negative radical, strongly suggest that the change of energy levels resulting in new regions of absorption and in luminescence is associated with energy changes in the negative radical brought about by the interaction of the adsorbed molecule with the solid surface.

The onset of a rapid fall of luminescence with liquid concentration at a point corresponding to only a fraction of a monomolecular layer in the case of silica wetted with water indicates that all the surface is not equally effective in bringing about these energy changes, and provides evidence from this new angle of the existence of active sites. The apparent difference in the number of active sites on the surface of the same solid, as demonstrated by the results of water and alcohol on silica, suggests that the number of active sites depends on the molecule adsorbed. It was observed during these studies that prolonged heating of a solid permanently reduced the brightness of luminescence obtainable by wetting. This result is in keeping with the well-known fact that prolonged heating often partially destroys the adsorptive and catalytic power of solids, presumably by a reduction of the surface area and number of active sites. In this connection it is perhaps worthy of note that of two Kieselguhrs, the more catalytically active was strikingly more luminescent when wetted.

Further evidence that all the active sites on a given solid are not alike is afforded by some observations on the luminescent spectra of wetted silica at three different water concentrations. When the water concentration is reduced to a value corresponding to the occupation of only 1/25 of the solid surface the peak of the main emission band is at 4000 A. At a concentration corresponding on the above views to the occupation of all the active sites (one quarter of the surface covered) the peak is at 4339 A., while at a concentration equivalent to five adsorbed layers of water molecules there is only a very slight further shift of the peak (to 4369 A.). Photometer records of the three spectrograms are shown in Figure 7. If the first occupied sites are the most active, as would be expected, the molecules attached to these would be expected to suffer the greatest energy changes from the normal state. This means that the normal absorption which has been modified by adsorption to give an abnormal absorption at the excitation peak of 3130 A. must be on the red side. The nearest absorption band of water on the red side appears to be at 5722 A. (weak) and the so-called rain bands at 5924 A. and 5952 A. Assuming that the end state in both cases is the same (e.g. one of pre-dissociation) the shift of absorption would involve an energy change in the water molecule of approximately 42 kgm. calories per mole. The heat of wetting of water on silica is about 15 kg. calories per mole. This, however, is the integrated value, that is, the mean value including molecules added long after all the active sites have been occupied. The heat evolved for the first molecules added at the most active sites is almost certainly much greater, so that although the value of the energy change corresponding to the shift of absorption from the 5924 A./5952 A. region to 3130 A. is nearly three times the integrated heat of wetting, it is not inconceivable that it does represent the heat of adsorption of the molecules adsorbed on the most active sites.

A much simpler interpretation is suggested by the fact that the free $-OH$ radical has a strong absorption band stretching from 2600 A. to 3470 A. with a peak at 3064 A. The similarity between this peak and the activation peak of

the luminescence of wetted silica suggests that the water molecules first adsorbed may be attached by a hydrogen bridge leaving an almost free $-OH$ radical. The similarity of the spectra of hydroxy molecules having different positive radicals adsorbed on the same solid indicates that this is the more likely explanation.

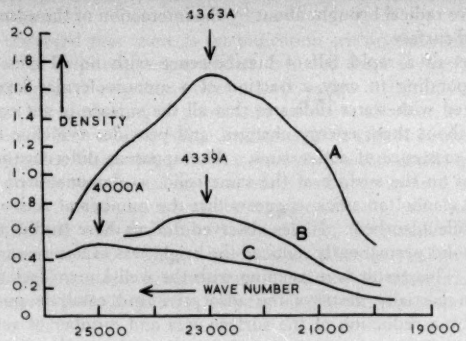


Figure 7. Photometer records of fluorescence spectrograms of silica wetted with water at various surface concentrations (specimen at 90° K.).
Curve A. Surface covered by five layers of water molecules.
Curve B. $\frac{1}{4}$ of the surface covered by water molecules.
Curve C. 1/25 of the surface covered by water molecules.

We can offer no explanation of the phosphorescence, visible in some cases for seconds and even minutes after excitation has ceased. The fact, at least in the case of water on silica, that the phosphorescence is approaching its maximum value at a coverage of the surface corresponding to far less than a monomolecular layer indicates the existence of metastable levels of astonishingly long life in single molecules or ions.

ACKNOWLEDGMENTS

It is a pleasure to thank Professor R. Whiddington, F.R.S., C.B.E., for his advice and for the laboratory facilities so freely made available. One of us (G.C.F.) is indebted to the Department of Scientific and Industrial Research for a Research Grant and some of the apparatus was purchased from funds provided by the Government Grant Committee of the Royal Society.

REFERENCES

DE BOER, J. H., 1935, *Electron Emission and Adsorption Phenomena*, p. 181 (Cambridge : University Press).
BOWEN, E. J., 1935, *J. Chem. Soc.*, 76.
BRUNAUER, S., 1944, *Physical Adsorption of Gases and Vapours*, p. 274 (Oxford : University Press).
BRUNAUER, S., EMMETT, P. H., and TELLER, E., 1938, *J. Amer. Chem. Soc.*, **60**, 309.
EWLES, J., 1930, *Nature, Lond.*, **125**, 706.
EWLES, J., and MARTIN, W. E., 1939, *Proc. Leeds Phil. Soc.*, **3**, Part X, 557.

# The Resolving Power and Intensity Relationships of the Fabry Perot Interferometer with Silvered Reflecting Surfaces

By R. J. BRIGHT, D. A. JACKSON and H. KUHN
Clarendon Laboratory, Oxford

*MS. received* 30*th September* 1948

*ABSTRACT.* By the use of a Fabry Perot etalon with very small spacing, the widths of the interference fringes were measured under conditions where the light could be considered as practically monochromatic. In this way, the resolving power which can be achieved with silver deposits of known optical density was determined for light of five different wavelengths between 6438 and 3610 A. The results can be used for selecting the most favourable thickness of silvering of etalon plates, namely that which gives the resolving power required for a given purpose without unnecessary loss of intensity. The application of the results to multiple etalons is discussed.

## § 1. INTRODUCTION

THE performance of the Fabry Perot interferometer depends largely on the optical properties of the partially reflecting metal coatings. For an instrument with perfectly plane, parallel and uniform surfaces, the intensity distribution is described by Airy's formula

$$I(\epsilon) = \frac{I_{\max}}{1 + F \sin^2 \pi\epsilon} \qquad \ldots\ldots(1)$$

where $\epsilon$ is the fraction of a wavelength by which the path difference between two successive rays is in excess of a whole number.

The intensity distribution within the fringes is determined by $F$, which depends only on the reflectivity $R$ according to the relation

$$F = 4R/(1-R)^2 \qquad \ldots\ldots(2)$$

where $R$ is defined as the intensity of the reflected light relative to that of the incident light. Thus the resolving power of an ideal etalon of given spacing depends only on $R$.

The absolute intensity, however, is determined by the factor $I_{\max}$ in equation (1), which is given by the relationship

$$I_{\max} = T^2/(1-R)^2 \qquad \ldots\ldots(3)$$

and thus depends also on the transmissivity $T$ of the surface, defined by the ratio of the intensities of transmitted and incident light. It will be assumed throughout that the optical properties of the two reflecting surfaces of the etalon are equal.

In the ideal case of a surface without absorption, for which the relation $R+T=1$ holds, $I_{\max}$ is equal to 1. The intensity at the maxima is then equal to the intensity of illumination which would be observed if the etalon were removed altogether. The degree to which, in actual fact, the sum $R+T$ approaches unity can serve as a measure of the optical quality of the coating. For highly reflecting surfaces, variation of thickness affects the values of $R$ and $T$ in opposite senses; in fact the sum $R+T$ is found to be approximately constant for films as they are used in practice. If the thickness is made large enough, $1-R$ approaches a limiting value while $T$ continues to decrease. Thus, according to (2) and (3),

increase of the thickness of the metal film may only cause a small increase in $F$, and therefore in resolving power, but result in a serious loss in intensity. A correct balance of the two factors is important in most interferometric work, especially when two or more etalons are used in series. Even for silver, which is almost exclusively used in the visible range of the spectrum, very little is known about the reflectivities of partially transparent films.

The measurements described below were made in order to establish the relationship between $R$ and $T$ for silver films produced by evaporation, for a range of wavelengths from 6500 to 3400 A. Since it is easy to control the thickness of the film by measurement of $T$ during the evaporation, the data thus provided can be used for producing silver films of the required value of $R$, after a suitable value of the latter has been chosen as a compromise between resolving power and intensity.

The method of determining $R$ consisted in measurement of the widths of Fabry Perot fringes produced under such conditions that the radiation could be considered to be practically monochromatic.

## §2. THE PRODUCTION OF THE SILVER FILMS

The silver films were produced by evaporation *in vacuo*. This method is comparatively simple and reliable and has generally superseded the method of cathodic sputtering, though under carefully chosen conditions this latter also seems to be able to give silver films of high performance. If the target surface is well cleaned and a high vacuum maintained during the evaporation, reproducible and very high values of the reflectivity $R$ can be achieved for any given transmission $T$, i.e. for any given thickness.

The evaporation chamber used in this work was a cylindrical brass tank of length 60 cm. and diameter 20 cm., evacuated by a large aperture mercury diffusion pump fitted with a liquid air trap to freeze out mercury. The vacuum was measured with a Pirani gauge. Three tungsten filaments, each of which carried two beads of pure silver, could be heated independently. This made it possible to stop the heating of each bead before it had completely evaporated. A few turns of fine platinum wire wrapped round the tungsten were used as a well-known method of making the silver adhere to the filaments. A shutter which could be placed between filament and target protected the latter from impurities evaporating from the filament in the early stages of heating. Another shutter, made of mica, prevented the front window from being covered with silver. Both shutters were operated by ground joints passing through the front lid. The vacuum seal between the latter and the chamber was made by means of a sulphur free rubber washer greased with apiezon tap grease.

Windows in the front and back plates allowed light from a lamp behind the tank to pass through the etalon plate *in situ* and to fall on a photocell. Colour filters were used to define the wavelength of the light. In this way the thickness of the silver film could be controlled during the evaporation by means of the measurement of the optical density.

The etalon plates were cleaned with strong nitric acid, rinsed with tap water and dried with pure cotton wool. The final cleaning was done in the tank by ionic bombardment; when a sufficiently good vacuum had been reached, a small amount of air was admitted and a glow discharge was passed through the tank for a few minutes. When a good vacuum had been established again the evaporation was carried out.

## § 3. THE MEASUREMENT OF THE TRANSMISSION

After the etalon plate had been taken out of the evaporation chamber, the transmission was measured more accurately for four narrow ranges of wavelengths in the visible spectrum. The etalon plate, placed face downward over a barrier layer "Eel" photocell, was illuminated by the light from a tungsten filament lamp fitted with suitable filters. The photo-current was measured with a low resistance galvanometer. This arrangement showed linear characteristics, and thus the transmission was given by the ratio of the current with the etalon plate in position to that with the plate removed. The filters used consisted of a copper sulphate filter to cut out all light of wavelength greater than 7000 A. and transmitting only 10% at 6500 A., and Wratten filters, according to Table 1.

Table 1

| Colour | orange | yellow | green | blue |
|---|---|---|---|---|
| Catalogue number | 27 | 22 + 58 | 62 | 47 |
| Mean wavelength (A.) | 6000 | 5700 | 5300 | 4400 |

The transmission at 3600 A. was measured by means of the light from a commercial mercury arc lamp, the bulb of which incorporated a Wratten filter 18a.

For two silverings, measurements of $T$ were also made at 3380 A. by photographic photometry. A quartz spectrograph was used and the transmission was measured for the silver line 3380 A.; for the intensity marks the continuous radiation from a hydrogen discharge was photographed with varying slit widths.

The accuracy of the transmission measurements for visible light was to within about $\pm 0{\cdot}005$ in the value of $T$, which was sufficient for the present purpose. The measurement of $T$ was always repeated at least once, after several days or weeks, and never showed any change.

## § 4. INTERFEROMETER AND LIGHT SOURCES

The width of interference fringes generally depends on the actual line width of the incident radiation, caused by Doppler effect, hyperfine structure and other causes of broadening, and on the "instrumental" width, i.e. the width which would be observed with strictly monochromatic light. If an etalon with very small spacing is used, and sufficiently narrow spectral lines are chosen, the width of the fringes is almost entirely due to the instrumental width. This condition was aimed at in the experiments described here.

An etalon with a separation of 1 mm. was used, so that one order corresponded to a wave-number difference of 5 $cm^{-1}$. Three U-shaped loops of tungsten wire were used as spacers. They were arranged so that the ends which were distorted when the wire was cut projected clear of the surface of the etalon plates. The pair of plates which was used throughout was made by Messrs. Adam Hilger Ltd. and consisted of quartz, cut at right angles to the optic axis. Their diameter was 2·5 cm., the thickness 0·7 cm., and the two faces formed an angle of 2′.

The spacers, owing to their small area of contact, responded readily to variations of the pressure of the adjustment springs. This had the advantage that the diameter of the central fringe could be made small enough to allow a very accurate adjustment of the parallelism of the plates. The radius of the central fringe was thus adjusted so that it corresponded to a difference of about 1/20 wavelength from that at the centre of the fringe system. Variations in this radius could be

kept down to less than one quarter of its value over the whole area of the etalon illuminated through the stops used (5 to 10 mm. in diameter). The accuracy of the adjustment was thus less than 1/40 of a wavelength. This limit was set more by the irregularities in the surfaces of the plates than by the method of adjustment.

With the small distances used, the thermal expansion of the spacers did not present any difficulty. Moreover, the optical system was situated in a room the temperature of which was thermostatically controlled to 1/10° C., while the light sources were in another room, the light being admitted through a small hole in the dividing wall.

The optical system consisted of a Hilger E2 quartz spectrograph (f = 60 cm.) and an external etalon mounting. An image of the light source was formed in the plane of the etalon, and a quartz fluorite achromat of focal length 33 cm. formed the interference fringes on the slit of the spectrograph.

The spectrograph, which was slightly astigmatic, was focused for the whole spectral range for horizontal focal lines. The correct setting of the achromat was found by tilting the etalon and finding the best focus for the narrow outer fringes. In the visible spectrum, an alternative method was employed as a check. A telescope fitted with crosswires was focused for "infinity"; the eye piece was then removed and the telescope placed in the position normally occupied by the etalon, with the objective facing towards the quartz-fluorite achromat, so that an image of the crosswire, illuminated by the light source, was formed on the plate. The setting of the achromat giving the best horizontal focus was then chosen. The method is very accurate for etalons of not too large aperture.

Two light sources were used, a commercial cadmium discharge lamp and a water cooled hollow cathode tube, lined with silver foil and operated at a current of about 100 ma. The discharge was carried by helium circulating through charcoal cooled in liquid air.

Table 2 contains a list of the lines used. The second column gives the ratio of wavelength to the half-value width due to Doppler effect, at an estimated temperature of 250° C. in the cadmium lamp and 50° C. in the hollow cathode tube. The last column shows the fraction of an order of an etalon of separation 1 mm. which corresponds to a difference of wavelength equal to this half-value width.

Table 2

| Line | $\lambda/d\lambda$ | $dn$ | Line | $\lambda/d\lambda$ | $dn$ |
|---|---|---|---|---|---|
| Cd 6438 | $6\times10^5$ | 0·005 | Cd 3610 | $6\times10^5$ | 0·009 |
| Ag 5465 | $8\times10^5$ | 0·004 | Cd 3438 | $6\times10^5$ | 0·009 |
| Cd 4662 | $6\times10^5$ | 0·007 | Ag 3380 | $8\times10^5$ | 0·008 |
| He 3888 | $1{\cdot}6\times10^5$ | 0·03 | | | |

With the exception of He 3888, the Doppler width of all the lines is less than 1/100 order. Broadening of the fringes due to this spectral width would therefore be relatively unimportant; only the measurements at 3888 A. may have been liable to a small systematic error.

The only lines having hyperfine structure are the last three in the table. The ultraviolet Cd lines possess two components on either side of the main lines, but they are too weak to have much effect. The hyperfine structure of the line 3380 of silver is about ten times smaller than the width of the fringes observed at this wavelength.

## § 5. PHOTOMETRIC MEASUREMENT OF THE FRINGES

The tilt of the etalon was so adjusted that the centre of the fringe system was inside the slit image, and that one fringe was visible on both sides of the centre. The half value width was determined from the first fringe and in many cases checked by the use of the second. The scale, near the first fringe, was generally about 7 mm. per order, a half value width of 1/20 order corresponding to about 0·3 mm. The grain of the plates (Ilford Astra III and Zenith) and development effects were therefore of no significance.

For the photometric measurements of the plates, the recording microphotometer at the Oxford University Observatory was kindly made available by Professor Plaskett. The resolving power of this instrument is largely determined by the size of the thermocouple, the image of which on the plate is 1/50 mm. A ratio of 7 : 1 of record scale to plate scale was used. Any inaccuracies arising from photographic or photometric effects were therefore well under 1/100 of an order.

Intensity marks were made on the same plate, but with a different spectrograph, of focal length 150 cm. The slit was illuminated uniformly with light from a tungsten filament or a hydrogen discharge tube, and exposures of equal duration were made with different widths of the slit.

The somewhat laborious nature of the direct photometric measurement of the widths of the fringes made it difficult to deal with a larger number of plates. A relative method was therefore also employed and proved to be reliable and more convenient.

If a Wollaston prism is interposed between the quartz fluorite achromat and the slit, with its refracting edges horizontal, the fringe system is doubled. Photographs were made with a number of different separations of these doubled fringes, by altering the distance of the Wollaston prism from the slit. (When the Wollaston prism was used, the distance of the achromat was, of course, changed to compensate the change in optical distance.) Visual inspection showed which of these doubled fringes had a separation equal to the half value width, or to some known fraction of it. Measurement of the outer, narrow fringes enabled the splitting caused by the Wollaston prism to be measured accurately.

This visual method was "calibrated" by making a sample plate showing the appearance of double fringes of various degrees of separation. The half value width of the fringes photographed without Wollaston prism was first measured by direct photometry; the Wollaston prism was then inserted and, by variation of its position, a series of double fringes of various known splittings was photographed. The intensity at the minimum, relative to that at the maxima, was calculated by a graphical method and also, as a check, measured photometrically (Table 3).

Table 3

| | | | | | | |
|---|---|---|---|---|---|---|
| Separation as fraction of half value width | | 0·63 | 0·75 | 0·90 | 1·1 | 1·25 |
| Intensity of minimum | calculated | 1·0 | 0·94 | 0·85 | 0·75 | 0·67 |
| | measured | — | 0·93 | 0·88 | 0·76 | 0·65 |

A separation of 0·75 of the half value width is still observable as resolved, and the greater resolutions are easily recognizable.

By visual comparison with this sample plate, the separation as a fraction of the half value width could be judged with sufficient accuracy from the use of Table 3, and the half value width could thus be calculated. The various fringes in each

exposure and the various exposures taken with different splittings allowed a number of comparisons covering different stages of resolution of these "doublets" with splittings ranging from 0·7 to 1·0 of the half value width. From each "doublet" the half value width was estimated and the average taken.

A difficulty of this double image method arose from the fact that the two fringes of a "doublet" were generally not of equal intensity, owing to polarization effects in the spectrograph. This was overcome by introducing a tilted glass plate causing partial polarization of the incident light. Small inequalities in the intensities were found not to impair the accuracy of the method.

## §6. RESULTS OF THE MEASUREMENTS OF TRANSMISSION

Table 4 gives the values of the transmission $T = I/I_0$ and the optical density $D = -\log T$ for the five silver coatings used. Each point is the average of two measurements. If an exponential law of absorption holds, the ratio of the optical densities of any two films should be independent of the wavelength. This is, on the whole, confirmed by the approximate agreement of all the values in any one of the last three lines of Table 4, where the suffix refers to the number of the silver

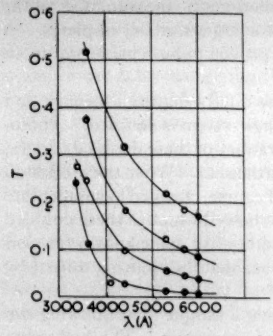


Figure 1.

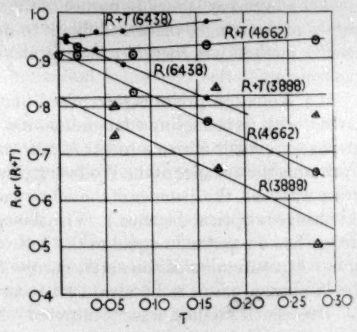


Figure 2.

coating. There seems, however, to be a slight rise of the ratio with increasing frequency. Interference effects inside the silver film might be responsible for these small deviations from Beer's law. The values of $T$ for the first four films are plotted in Figure 1.

## §7. WIDTH OF FRINGES AND REFLECTIVITY

Table 5 contains the half value widths $\delta$, expressed as fractions of an order, of the fringes produced by etalons with the five different silverings. The results obtained from each photograph are given separately. The figures in brackets after the half value widths found by the method of the double image, indicate the degree of resolution in the photograph from which this half value width has been deduced; e.g. "0·43 (0·8)" signifies that the degree of resolution was 0·8 of that corresponding to the separation equal to the half value width, and that the value of (separation/0·8) is equal to 0·43.

Table 4

| Wavelength (A.) | | 6000 | 5700 | 5300 | 4400 | 4100 | 3600 | 3380 |
|---|---|---|---|---|---|---|---|---|
| Film No. | | | | | | | | |
| 7 | *T* | 0·17 | 0·19 | 0·22 | 0·32 | | 0·52 | |
| | *D* | 0·77 | 0·72 | 0·66 | 0·50 | | 0·28 | |
| 3 | *T* | 0·086 | 0·100 | 0·120 | 0·182 | | 0·37 | |
| | *D* | 1·065 | 1·00 | 0·92 | 0·74 | | 0·43 | |
| 4 | *T* | 0·040 | 0·045 | 0·053 | 0·097 | | 0·24 | (0·27) |
| | *D* | 1·40 | 1·35 | 1·28 | 1·01 | | 0·62 | (0·57) |
| 5 | *T* | 0·008 | 0·010 | 0·011 | 0·027 | 0·030 | 0·114 | (0·24) |
| | *D* | 2·10 | 2·00 | 1·96 | 1·57 | 1·52 | 0·96 | (0·62) |
| 6 | *T* | | | | 0·005 | | 0·04 | |
| | *D* | | | | 2·3 | | 1·4 | |
| $D_3 : D_7$ | | 1·39 | 1·39 | 1·39 | 1·48 | | 1·54 | |
| $D_4 : D_3$ | | 1·31 | 1·35 | 1·39 | 1·37 | | 1·44 | |
| $D_5 : D_4$ | | 1·50 | 1·48 | 1·53 | 1·55 | | 1·55 | (1·1) |

Table 5. Half Value Widths δ of Fringes as Fractions of Order

| Film No. | Method * | 6438 | 5465 | 4662 | 3888 | 3610 | 3438 | 3380 A. |
|---|---|---|---|---|---|---|---|---|
| 7 | D.I. | 0·068 (1·0)<br>0·064 (0·7) | | 0·135 (1·0) | 0·25 (1·0)<br>0·25 (0·7) | | | |
| | Ph. | 0·065<br>0·058 | 0·10 | 0·14<br>0·14 | | | | |
| 3 | D.I. | 0·039 (0·9) | 0·067 (1·0) | | | | | |
| | Ph. | 0·036 | 0·070 | 0·085 | 0·20 | | | |
| 4 | D.I. | 0·028 (0·9)<br>0·028 (0·7) | 0·043 (0·8) | 0·055 (0·9)<br>0·061 (0·7) | | 0·18 (0·9) | | |
| | Ph. | 0·023 | 0·036 | 0·063<br>0·061 | 0·13 | | 0·30 | |
| 5 | D.I. | 0·021 (1·0)<br>0·021 (0·8)<br>0·021 (1·0) | | 0·027 (1·0)<br>0·027 (0·8)<br>0·029 (1·0)<br>0·029 (0·8)<br>0·029 (0·7)<br>0·032 (0·8)<br>0·032 (1·0) | 0·10 (1·0)<br>0·10 (0·8)<br>0·10 (0·7)<br>0·10 (1·0)<br>0·10 (0·9)<br>0·10 (0·9) | 0·10 (0·9)<br>0·10 (0·7)<br>0·10 (1·0)<br>0·12 (0·7)<br>0·12 (0·9) | | 0·20 (1·0)<br>0·20 (0·85)<br>0·20 (0·7) |
| 6 | D.I. | | | 0·030 (1·2) | | 0·10 (1·0)<br>0·11 (1·1)<br>0·10 (1·0)<br>0·10 (0·7)<br>0·10 (0·9) | | |

* D.I. = double image method; Ph. = direct photometric method.

The good agreement between the values obtained by the method of the double image with different degrees of resolution, and the agreement of these values with those found by direct photometric measurement shows that the method of measurement is sufficiently accurate.

The first two lines in each section of Table 6 give the transmissivities $T$ read from the curves of Figure 1, and the mean values of the half value widths $\delta$, as fractions of an order, derived from Table 5.

Table 6

| | | 6438 | 5465 | 4662 | 3888 | 3610 A. |
|---|---|---|---|---|---|---|
| 7 | $T$ | 0·16 | 0·21 | 0·28 | 0·43 | |
| | $\delta$ | 0·064 | 0·10 | 0·14 | 0·25 | |
| | $R$ | 0·82 | 0·73 | 0·66 | 0·46 | |
| | $T+R$ | 0·98 | 0·94 | 0·94 | 0·89 | |
| 3 | $T$ | 0·07 | 0·11 | 0·16 | 0·28 | |
| | $\delta$ | 0·037 | 0·068 | 0·085 | 0·20 | |
| | $R$ | 0·89 | 0·81 | 0·77 | 0·50 | |
| | $T+R$ | 0·96 | 0·92 | 0·93 | 0·78 | |
| 4 | $T$ | 0·04 | 0·05 | 0·08 | 0·17 | 0·24 |
| | $\delta$ | 0·026 | 0·039 | 0·060 | 0·13 | 0·18 |
| | $R$ | 0·92 | 0·89 | 0·83 | 0·67 | 0·58 |
| | $T+R$ | 0·96 | 0·94 | 0·91 | 0·84 | 0·82 |
| 5 | $T$ | 0·007 | | 0·02 | 0·06 | 0·11 |
| | $\delta$ | 0·021 | | 0·029 | 0·10 | 0·11 |
| | $R$ | 0·94 | | 0·91 | 0·74 | 0·72 |
| | $T+R$ | 0·95 | | 0·93 | 0·80 | 0·83 |
| 6 | $T$ | | | 0·00 | | 0·04 |
| | $\delta$ | | | 0·030 | | 0·10 |
| | $R$ | | | 0·91 | | 0·74 |
| | $T+R$ | | | 0·91 | | 0·78 |

The formulae (1) and (2) lead to a relation between half value width $\delta$ and reflectivity $R$:

$$\sin \pi\delta/2 = (1-R)/(2\sqrt{R}).$$

This relation has been used for calculating the second line of Table 7, and also for calculating the values of $R$ in the third rows of Table 6 from the measured values of $\delta$ given in the second rows. Figure 2 shows a plot of these values of $R$ against $T$. To avoid confusion of the graph, the data for 5465 and 3610 A. have been omitted.

## §8. RESOLVING POWER AND INTENSITY

If two monochromatic radiations of equal intensity differ in wavelength by an amount $d\lambda$ such that the etalon fringes are separated by their half value width, the resulting intensity curve can be derived from Airy's formula. The ratio of the intensity of the maxima to that of the minimum between them is found as

$$1 + \frac{1}{1+4R(\sin^2 \pi\delta)/(1-R)^2},$$

where $\delta$ is the fraction of an order corresponding to the half value width and is the function of $R$ quoted in § 7. For small values of $\delta$ this quantity is independent of the value of $R$ and is equal to 1·20. The dip in the intensity curve is thus very similar to that produced in a prism or grating spectrograph by two lines fulfilling Rayleigh's criterion of resolution, as appears also from the values of Table 3. It is therefore convenient to define the limits of resolution by the condition $n\lambda=(n-\delta)(\lambda+d\lambda)$ which gives the resolving power $\lambda/d\lambda=n/\delta=2t/\lambda\delta$, where $n$ is the order of interference and $t$ the separation between the plates. The value $1/\delta$ can be considered as "effective number of interfering beams", $N_{\text{eff}}$, from which the resolving power is obtained by multiplication with the order of interference. In Figure 3, this value is plotted as a function of $T$ from the values of Table 5.

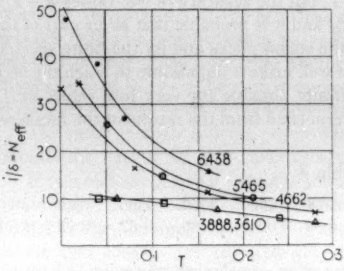


Figure 3.

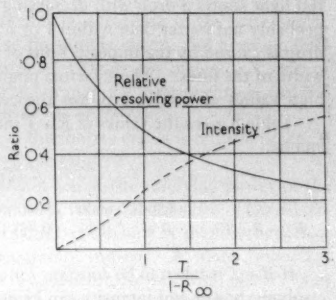


Figure 4.

The "contrast" of the fringes for monochromatic light, i.e. the ratio of the intensity of the maxima to that of the minima (the background at a point midway between two maxima) can be derived from $R$:

$$I_{\max}/I_{\min}=(1+R)^2/(1-R)^2.$$

This "contrast" factor is also included in Table 7. It is an important factor whenever weak components are to be observed in the presence of strong lines.

The intensity of the maxima, relative to the intensity of illumination in the absence of an etalon depends on both $R$ and $T$, according to equation (3).

Table 7

| $R$ | 0·98 | 0·975 | 0·97 | 0·96 | 0·95 | 0·94 | 0·93 | 0·92 | 0·91 | 0·90 | |
|---|---|---|---|---|---|---|---|---|---|---|---|
| $1/\delta$ | 155 | 134 | 104 | 77 | 62 | 52 | 44 | 38 | 33 | 29 | |
| $I_{\max}/I_{\min}$ | 9800 | 6200 | 4300 | 2400 | 1500 | 1000 | 750 | 550 | 450 | 360 | |
| $R$ | 0·88 | 0·86 | 0·84 | 0·82 | 0·80 | 0·78 | 0·75 | 0·70 | 0·65 | 0·60 | 0·50 |
| $1/\delta$ | 24 | 20 | 18 | 16 | 14 | 12 | 11 | 9 | 7 | 6 | 5 |
| $I_{\max}/I_{\min}$ | 240 | 170 | 130 | 100 | 80 | 65 | 50 | 33 | 22 | 16 | 9 |

## § 9. USE OF THE DATA

On the basis of the data contained in Figures 1 and 3, Tables 4 and 6 and equation (3) it is possible (i) to decide upon a value of $T$ for the silver film which, for the given purpose, provides the best compromise between the requirements of

resolving power and intensity, and (ii) to achieve the required value of $T$ by controlling, during the evaporation, the optical density measured at any conveniently chosen wavelength.

For example, if a minimum $N_{\text{eff}}$ (resolving power/order) be required at a given wavelength, Figure 3 gives values of $T$ for neighbouring wavelengths, and the $T$ for the required wavelength is found by interpolation from Figure 1. The maximum intensity available is then calculated from equation (3).

The data may be presented in a way in which the parameter wavelength is artificially suppressed, thus reducing the complexity of the numerous curves for different wavelengths. In Figure 2, the sum of $R$ and $T$ is plotted against $T$ for different wavelengths. It appears that for practical purposes $R+T$ can be assumed to be independent of the thickness of the layer. Actually, the curve for red light shows a drop with decreasing $T$, but the accuracy of the values $R+T$ is probably not better than within 1 or 2%, and it is probable that all or part of the drop is caused by the imperfections of the etalon plates and by the finite spectral width of the lines. These factors might well make it impossible to reach the very high values of resolving power theoretically possible for very low values of $T$.

Table 8 gives the values of $R+T$ interpolated from the results of the measurements.

Table 8

| $\lambda$ (A.) | 6500 | 6000 | 5500 | 5000 | 4500 | 4000 | 3800 | 3600 | 3400 |
|---|---|---|---|---|---|---|---|---|---|
| $R_\infty = R+T$ | 0·97 | 0·96 | 0·95 | 0·94 | 0·92 | 0·86 | 0·82 | 0·78 | (0·70) |

If $R+T$ is taken to be constant for any given wavelength, the relation between resolving power and intensity can be graphically represented in the following way (Figure 4): The ordinate of one curve is the intensity of the maxima relative to the intensity in the absence of an etalon, that of the other curve is the resolving power expressed as a fraction of that for a very dense layer with reflectivity $R_\infty = R+T$ (change of wavelength is allowed for by change of the value of $R_\infty$). The abscissae of both curves are the values of $T/(1-R_\infty)$.*

The curves show, for example, that for $T = 1-R_\infty$ the resolving power is 50% of the maximum possible with a very dense silvering, and the intensity of the fringes is 25% of that in the absence of an etalon.

## §10. APPLICATION OF THE RESULTS TO MULTIPLE ETALONS

In work with the multiple etalon, a quantitative control of the thickness of the reflecting films is almost indispensable. In this instrument, which was first described by Houston (1927), two etalons are used in series, with spacings $t$ and $t'$ in an integral ratio. A method of adjustment by means of change of air pressure has been introduced by two of the present authors (Jackson and Kuhn 1938, 1939). The function of the shorter etalon, of spacing $t'$, consists mainly in suppressing certain orders of the large etalon and thus extending the spectral range of the latter. The reflectivity of the shorter etalon must therefore be made large enough to cause the subsidiary maxima (the suppressed orders) to be faint compared with the weakest line of the pattern under investigation. The ratio of the intensity of the principal maxima to that of the first, i.e. strongest, subsidiary maxima is

* The broken curve is the function $x^2/(x+1)^2$ of the abscissa $x$.

given by the relation $I/I' = 1 + 4R(\sin^2 \pi t'/t)/(1-R)^2$. Some typical values of this ratio have been calculated from the data of the preceding paragraphs for a silvering of the shorter etalon with $T = 0{\cdot}04$ at 6000 A. (Table 9).

Table 9

| $\lambda$ (A.) | 6500 | 6000 | 5500 | 5000 | 4500 | 4000 | 3800 |
|---|---|---|---|---|---|---|---|
| $t/t'$ | | | | | | | |
| 2 | 1000 | 750 | 400 | 200 | 140 | 40 | 20 |
| 4 | 500 | 380 | 200 | 100 | 70 | 20 | 11 |
| 10 | 100 | 70 | 40 | 20 | 15 | 5 | 4 |
| 20 | 25 | 18 | 11 | 6 | 4 | 2 | 1·5 |

The compound etalon with both components silvered to this density is very effective; the intensity of the principal maxima is, according to the wavelength, between 0·21 and 0·36 of that in the case of the simple etalon, and between 0·04 and 0·11 of that if the lines were photographed without any etalon. A ratio of the spacings of 10 : 1 can be used in the red and orange, for most purposes, and 4 : 1 is satisfactory over most of the visible part of the spectrum.

The small gain in resolving power due to the shorter etalon is of little practical importance, except for very small values of the ratio $t/t'$.

If two etalons of equal spacings are used in series, the resolving power of the combination is appreciably larger (by about 60% for equal densities of the silverings) than that of a single etalon. Full use of this fact can only be made if the phases of the two etalons are adjusted very accurately indeed. A more important application of this form of multiple etalon is its use for the detection of very faint components. The ratio of the intensity of the maxima to that at the point midway between them is clearly the product of the corresponding ratios for the individual etalons. If the values in the third line of Table 7 are squared, they give the values $I_{max}/I_{min}$ for the combination of two etalons of equal spacings and equal reflectivities of the silver films.

## § 11. DISCUSSION AND COMPARISON WITH DIRECT MEASUREMENTS OF REFLECTIVITIES

The intensity relations discussed in the last paragraph are only valid for strictly monochromatic light. If the "spectral" width of the line, which may for instance, be caused by Doppler broadening, is comparable with the instrumental width or even larger, the ratio $I_{max}/I_{min}$ is reduced correspondingly.

When the values of $R$ derived from widths of etalon fringes are compared with direct measurements of reflectivities, it must be remembered that Airy's formula cannot be expected to hold rigorously, owing to imperfections of the plates and the silver films, and that the value of $R$ thus derived may differ slightly from the actual reflectivity. This objection does not, of course, affect the relation between transmission and resolving power, both of which have been measured directly. It would, however, affect the intensity relations which then would only have approximate validity. The influence of imperfections on the intensity distribution has been discussed by Dufour and Picca (1945) but the experimental data for the contrast factor $I_{max}/I_{min}$ are too scarce to allow any definite conclusions.

It is fairly obvious that imperfections of the plates or silver films must increase

the half value width for a given reflectivity. The values of $R$ derived from widths of etalon fringes are therefore likely to be slightly lower than the reflectivities which accurate direct measurements of the same films would have given.

The only direct measurements of reflectivities of vacuum deposited transparent silver films described in the literature appear to be those by Strong and Dibble (1940). But they are relative values only, measured with reference to a thick silver film. For green light, Tolansky (1946) reports some values of $R$ and $T$ which are fairly close to our results, but no experimental details are given.

The reflectivity of thick silver films ($T=0$), deposited *in vacuo*, has been measured by Baxter (1937), who finds a value of 0·94 at 6000 A., and by Strong (1940) who finds 0·95 at the same wavelength. Edwards and Petersen (1936) measure reflectivities of thick films deposited under apparently specially good conditions. Their value of $R_\infty$ for yellow light is 0·985. In view of the mentioned influence of imperfections of the surfaces, this latter value is not incompatible with our results, whereas the values of Baxter and Strong seem to be rather low.

For films produced by cathodic sputtering, some extremely high values of $R+T$ have been reported by Romanowa, Robzow and Pokrowsky (1934), but it is not clear from the description of their method if infra-red light has been excluded. Measurements by Goos (1936), of reflectivities of sputtered films give considerably lower values, the sum $R+T$ being about 0·95 for 5780 A. and 0·92 for 4350 A.

## REFERENCES


Baxter, A., 1937, *J. Sci. Instrum.*, **14,** 303.
Dufour, C., and Picca, P., 1945, *Rev. d'Optique*, **24,** 19.
Edwards, H. W., and Petersen, R. P., 1936, *Phys. Rev.*, **50,** 871.
Goos, F., 1936, *Z. Phys.*, **100,** 95.
Houston, W. V., 1927, *Phys. Rev.*, **29,** 475.
Jackson, D. A., and Kuhn, H., 1938, *Proc. Roy. Soc.* A, **167,** 205; 1939, *Ibid.*, **173,** 278.
Romanowa, M., Robzow, A., and Pokrowsky, G., 1934, *Phys. Z. Sowjet*, **5,** 46.
Strong, J., 1940, *Mod. Phys. Lab. Practice*, pp. 185 and 375.
Strong, J., and Dibble, B., 1940, *J. Opt. Soc. Amer.*, **30,** 431.
Tolansky, S., 1946, *Physica*, **12,** 650.

# Intensity Distribution for Bands of the γ-System of $MgH^+$

By M. E. PILLOW
Imperial College, London, and Northern Polytechnic, London

*Communicated by R. W. B. Pearse*; *MS. received* 24*th May* 1948, *and in amended form* 7*th October* 1948

*ABSTRACT.* The intensity distribution for bands of the γ-system of $MgH^+$ is deduced theoretically from the wave functions for the various energy states, and is compared with the distribution of the observed bands.

Lines of the (2, 3) band, not previously noted, have been observed.

## § 1. INTRODUCTION

PEARSE (1929) has published particulars of a number of bands in the ultra-violet spectrum produced by a magnesium arc in hydrogen. These bands he attributes to a $^1\Sigma \rightarrow {}^1\Sigma$ transition for $MgH^+$. Guntsch (1934, 1939) later made further measurements on this sytem of bands, using as source a hydrogen discharge tube with magnesium electrodes, and also a magnesium-carbon arc, and carrying his investigations to longer wavelengths. His analysis agrees closely with that of Pearse, and he has observed a number of additional bands.

When the bands so measured are set out in the usual vibration table they are found to lie close to one main parabola, with a suggestion of the existence of an inner parabola (Table 1). The positions of these parabolas are indicated by heavy type.

Table 1. Observed Bands

| $v'$ \ $v''$ | 0 | 1 | 2 | 3 | 4 | 5 | 6 | 7 | 8 |
|---|---|---|---|---|---|---|---|---|---|
| 0 | AB | **AB** | **AB** | **AB** | B | | | | |
| 1 | **AB** | AB | | AB | B | **B** | | | |
| 2 | **AB** | | | **C** | | B | **B** | B | |
| 3 | **AB** | | | | **B** | | B | **B** | B |
| 4 | **B** | | | | | | | | **B** |
| 5 | B | | | | | | | | |
| 6 | | **B** | | | | | | | |

A: bands recorded by Pearse; B: bands recorded by Guntsch; C: band now observed (see § 8).

## § 2. SPECTROSCOPIC DATA AND FORMULAE USED

The vibrational energy terms are expressed in the form

$$G(v) = \omega_e(v+\tfrac{1}{2}) - x_e\omega_e(v+\tfrac{1}{2})^2 \ldots .$$

Pearse's analysis gives, for the two electronic states, initial state $\omega'_e = 1138{\cdot}4$, $x'_e\omega'_e = 9{\cdot}5$; final state $\omega''_e = 1702{\cdot}2$, $x''_e\omega''_e = 34{\cdot}2$.

The rotational terms are expressed in the form

$$F(J)=\{B_e-\alpha(v+\tfrac{1}{2})\ldots.\}J(J+1)+DJ^2(J+1)^2\ldots.$$

For these constants, Pearse gives: initial state, $B'_e=4{\cdot}302$, $\alpha'=0{\cdot}0492$; final state, $B''_e=6{\cdot}378$, $\alpha''=0{\cdot}1854$. The $D$'s are too small to be relevant here. The corresponding values of the constants as calculated by Guntsch in 1934 from his measurements agree closely with these, except in the case of $x''_e\omega''_e$, for which he gives 30·2, and suggests an appreciable term in $(v''+\frac{1}{2})^3$. Pearse's values have been used in the following calculations.*

## § 3. POTENTIAL ENERGY FUNCTIONS AND DERIVED CONSTANTS

The polynomial expansion in powers of $(r-r_e)/r_e$, with coefficients calculated from Dunham's results (1932), was found unsatisfactory for both electronic states, as the coefficients are too large to allow the polynomials to converge suitably. Morse's form of the potential function (1929) has therefore been used, $U=\mathbf{D}(1-e^{-ax})^2$, where $x$ stands for $(r-r_e)$. The constants in this equation are derived from the spectroscopic constants :

$$\mathbf{D}=\omega_e^2/4x_e\omega_e; \quad a=\sqrt{(8\pi^2c\mu x_e\omega_e/h)}; \quad B_e=h/8\pi^2c\mu r_e^2, \quad \text{giving } r_e;$$

$$\mu=(24{\cdot}32/25{\cdot}32)\times 1{\cdot}66\times 10^{-24}=1{\cdot}595\times 10^{-24}\ \text{gm.}$$

whence $r'_e=2{\cdot}012\times 10^{-8}$ cm., $r''_e=1{\cdot}652\times 10^{-8}$ cm.; $\mathbf{D}'=34{,}110\ \text{cm}^{-1}$,

$$\mathbf{D}''=21{,}180\ \text{cm}^{-1}; \quad a'=0{\cdot}7384\times 10^8\ \text{cm}^{-1}, \quad a''=1{\cdot}401\times 10^8\ \text{cm}^{-1}.$$

The curves plotted from these data are shown in the Figure, together with the parabolic curves (dotted) obtained by using only the first term, $\mathbf{D}a^2x^2$, of the expansion in each case.

Rees (1947) suggests a method of plotting the potential curve directly in terms of the measured constants. This method was applied here, and was found to give curves for both states agreeing very closely with those derived from the Morse function.

[It should be noted that the values $\mathbf{D}'$, $\mathbf{D}''$ quoted above give values for the dissociation energies of 4·13 ev. and 2·5 ev., and these are probably high, being derived by extrapolation from the data for a few bands. In particular, the difference $\mathbf{D}'_e-\mathbf{D}''_e$ is much greater than that obtained by considering the $^2P\rightarrow{}^2S$ transition for ionized magnesium. But the potential curves are used only over the range covered by the measured bands, and they are presumably reasonably correct within this range.]

## § 4. WAVE FUNCTIONS FOR VIBRATOR

To avoid the heavy working involved in the calculation of the wave functions from Morse's formula, the curves have been derived by approximation from those for a harmonic oscillator, given by

$$\psi_v=d^{-\frac{1}{2}}(2^v v!\sqrt{\pi})^{-\frac{1}{2}}\exp\{-\tfrac{1}{2}(x/d)^2\}H_v(x/d),$$

where $d^2=h/4\pi^2c\mu\omega_e$. Gaydon and Pearse (1939) give a table of these functions, omitting the initial $d^{-\frac{1}{2}}$, for half-integral values of $x/d$. For the higher energy levels it has been found necessary to calculate some intermediate values, and the complete scheme used is shown in Table 2.

* Guntsch, in his dissertation in 1939, to which the author had access only after making these calculations, introduces a term in $(v+\frac{1}{2})^3$ in the excited state also, and this necessitates a change in $x'_e\omega'_e$ to 6·8. Over the small range of energy levels involved, however, the difference produced by this change of constants is small, and the effect on the calculated intensities negligible.

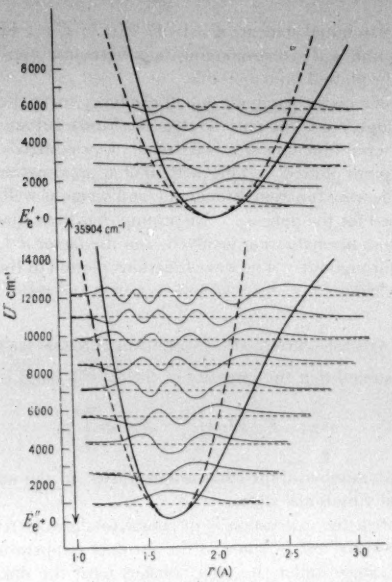


Potential energy functions and wave functions for vibrations in two electronic states.

Table 2. Wave Functions Corresponding to Parabolic Potential Energy Function

| $x/d$ | $n$ | 0 | 1 | 2 | 3 | 4 | 5 | 6 | 7 | 8 |
|---|---|---|---|---|---|---|---|---|---|---|
| 0 | | 0·751 | 0 | −0·531 | 0 | 0·460 | 0 | −0·420 | 0 | 0·393 |
| ¼ | | | | | −0·302 | 0·336 | 0·323 | −0·261 | −0·334 | 0·128 |
| ½ | | 0·663 | 0·469 | −0·234 | −0·478 | 0·034 | 0·438 | 0·096 | −0·380 | −0·184 |
| ¾ | | | | | −0·460 | −0·287 | 0·279 | 0·382 | −0·102 | −0·395 |
| 1 | | 0·456 | 0·644 | 0·322 | −0·263 | −0·465 | −0·056 | 0·391 | 0·263 | −0·234 |
| 1¼ | | | | | 0·027 | −0·420 | −0·360 | 0·124 | 0·416 | 0·144 |
| 1½ | | 0·244 | 0·518 | 0·604 | 0·317 | −0·187 | −0·461 | −0·229 | 0·243 | 0·397 |
| 1¾ | | | | | 0·513 | 0·125 | −0·321 | −0·430 | −0·106 | −0·310 |
| 2 | | 0·101 | 0·287 | 0·502 | 0·585 | 0·393 | −0·026 | −0·389 | −0·393 | −0·028 |
| 2¼ | | | | | 0·553 | 0·546 | 0·282 | −0·132 | −0·420 | −0·349 |
| 2½ | | 0·033 | 0·117 | 0·269 | 0·453 | 0·567 | 0·493 | 0·188 | −0·198 | −0·428 |
| 2¾ | | | | | 0·330 | 0·493 | 0·562 | 0·443 | 0·130 | −0·235 |
| 3 | | 0·008 | 0·035 | 0·100 | 0·217 | 0·373 | 0·513 | 0·549 | 0·405 | 0·094 |
| 3¼ | | | | | | | 0·401 | 0·522 | 0·536 | 0·366 |
| 3½ | | 0·002 | 0·008 | 0·027 | 0·071 | 0·153 | 0·275 | 0·415 | 0·522 | 0·526 |
| 3¾ | | | | | | | | | | 0·542 |
| 4 | | 0 | 0·001 | 0·005 | 0·017 | 0·043 | 0·093 | 0·177 | 0·292 | 0·418 |
| 4¼ | | | | | | | | | | |
| 4½ | | | 0 | 0·001 | 0·003 | 0·009 | 0·022 | 0·049 | 0·098 | 0·174 |
| 4¾ | | | | | | | | | | |
| 5 | | | | 0 | 0 | 0·001 | 0·004 | 0·009 | 0·022 | 0·045 |
| 5¼ | | | | | | | | | | |
| 5½ | | | | | | 0 | 0 | 0·001 | 0·003 | 0·008 |
| 5¾ | | | | | | | | | | |
| 6 | | | | | | | | 0 | 0 | 0·001 |

The values of $d$ in initial state are $d' = 1{\cdot}749 \times 10^{-9}$; $d'' = 1{\cdot}426 \times 10^{-9}$. Since $x = r - r_e$, the function $\psi_v d^{\frac{1}{2}}$ corresponding to a harmonic oscillator at any one energy level could be plotted from this table.

To each value of $r$ on the parabolic potential energy curve there corresponds a slightly different value, $r_M$, at the same level on the Morse curve. The necessary correction of the wave functions has been made approximately by using $r_M$ in place of $r$ for each point plotted. This method of approximation is rapid, gives a smooth curve for the wave function throughout, and seems as well justified as other approximations used for the purpose. No attempt has been made to correct the slight departure from normalization involved, and the factor $d^{-\frac{1}{2}}$, being constant, has been omitted throughout. The wave functions plotted in this way are shown in the Figure.

## § 5. CALCULATION OF INTENSITIES OF BANDS

It has been assumed that the intensity of the $(v', v'')$ band is proportional to

$$\exp(-E_{v'}/k\theta)\nu^4\left[\int_{-\infty}^{\infty}\psi'\psi''\,dr\right]^2,$$

where $\nu_0$ is the wave number of the band-origin and $\psi', \psi''$ the wave functions for the initial and final vibrational states.

The first factor in the expression is intended to allow for the effect on the distribution of the initial energy states of the absolute temperature $\theta$. This is a doubtful quantity, since under the high voltages used the disturbances in the molecular states are not due to thermal movements alone. It will be seen (§ 7) that the visibility of the measured bands indicates a value of $\theta$ probably in excess of the temperature actually possible in the tube. The integration has been carried out numerically, using the graphs of the wave functions, as was done by Gaydon and Pearse (1939).

## § 6. TABULATION OF INTENSITIES

Tables 3–6 show the calculated intensities for a series of values of $\theta$. The intensity in each case is expressed as a percentage of that of the strongest band, and anything below 1% is omitted. Thick type indicates the parabolas connecting calculated maxima.

No attempt could be made to compare the intensities experimentally, but it is presumed that those bands which have been observed are probably the most intense.

Table 3. Intensity Distribution for $\theta \to \infty$

| $v'$ \ $v''$ | 0 | 1 | 2 | 3 | 4 | 5 | 6 | 7 | 8 |
|---|---|---|---|---|---|---|---|---|---|
| 0 | **33**$^{AB}$ | **85**$^{AB}$ | **100**$^{AB}$ | **65**$^{AB}$ | **33**$^{B}$ | 7 | | | 1 |
| 1 | **71**$^{AB}$ | **46**$^{AB}$ | | **51**$^{AB}$ | **87**$^{B}$ | **69**$^{B}$ | 24 | 2 | 1 |
| 2 | **67**$^{AB}$ | 12 | 8 | **10**$^{C}$ | 4 | **78**$^{B}$ | **85**$^{B}$ | **46**$^{B}$ | 5 |
| 3 | **63**$^{AB}$ | 2 | **32** | 1 | **7**$^{B}$ | 1 | **42**$^{B}$ | **88**$^{B}$ | **66**$^{B}$ |
| 4 | **19**$^{B}$ | **21** | 14 | 8 | **23** | | 1 | 17 | **73**$^{B}$ |
| 5 | **31**$^{B}$ | **40** | | **14** | 1 | **31** | **22** | 3 | 11 |

Table 4. Intensity Distribution for $\theta = 3{,}000°$ K.

| $v'$ \ $v''$ | 0 | 1 | 2 | 3 | 4 | 5 | 6 | 7 | 8 |
|---|---|---|---|---|---|---|---|---|---|
| 0 | 33$^{AB}$ | **85**$^{AB}$ | **100**$^{AB}$ | **65**$^{AB}$ | 33 | 17 | | | 1 |
| 1 | **35**$^{AB}$ | 27$^{AB}$ | | 30$^{AB}$ | **50**$^{B}$ | **40**$^{B}$ | 14 | 1 | 1 |
| 2 | **22**$^{AB}$ | 4 | 3 | 3$^{C}$ | 1 | 26$^{B}$ | **29**$^{B}$ | 15$^{B}$ | 2 |
| 3 | **12**$^{AB}$ | | **6** | | **1**$^{B}$ | | 8$^{B}$ | **17**$^{B}$ | 13$^{B}$ |
| 4 | 2$^{B}$ | 2 | 2 | 1 | **3** | | | 2 | **8**$^{B}$ |
| 5 | 1$^{B}$ | **3** | | 1 | | **2** | 1 | | |

Table 5. Intensity Distribution for $\theta = 2{,}000°$ K.

| $v'$ \ $v''$ | 0 | 1 | 2 | 3 | 4 | 5 | 6 | 7 | 8 |
|---|---|---|---|---|---|---|---|---|---|
| 0 | 33$^{AB}$ | **85**$^{AB}$ | **100**$^{AB}$ | 65$^{AB}$ | 33$^{B}$ | 7 | | | 1 |
| 1 | **27**$^{AB}$ | 20$^{AB}$ | | 23$^{AB}$ | **38**$^{B}$ | **30**$^{B}$ | 11 | 1 | |
| 2 | **13**$^{AB}$ | 2 | 2 | 2$^{C}$ | 1 | 15$^{B}$ | **17**$^{B}$ | **9**$^{B}$ | 1 |
| 3 | **5**$^{AB}$ | | 3 | | 1$^{B}$ | | 4$^{B}$ | **8**$^{B}$ | **6**$^{B}$ |
| 4 | **1**$^{B}$ | 1 | | | 1 | | | | **3**$^{B}$ |
| 5 | | 1 | | | | | | | |

Table 6. Intensity Distribution for $\theta = 1{,}000°$ K.

| $v'$ \ $v''$ | 0 | 1 | 2 | 3 | 4 | 5 | 6 | 7 | 8 |
|---|---|---|---|---|---|---|---|---|---|
| 0 | 33$^{AB}$ | **85**$^{AB}$ | **100**$^{AB}$ | **65**$^{AB}$ | 33$^{B}$ | 7 | | | 1 |
| 1 | **12**$^{AB}$ | 9$^{AB}$ | | 10$^{AB}$ | **17**$^{B}$ | **13**$^{B}$ | 5 | | |
| 2 | 2$^{AB}$ | | | | | 3$^{B}$ | 3$^{B}$ | 2$^{B}$ | |
| 3 | | | | | | | | 1$^{B}$ | |

A: bands observed by Pearse; B: bands observed by Guntsch; C: band now observed.

## §7. RESULTS

The calculated intensities at any temperature from 1,000° K. upwards show maxima lying on a definite outer parabola, with the (0,2) band strongest in every case, and at very high temperatures the inner parabola also appears. The values of $\theta$ required for all the recorded bands to be intense enough to be seen are very high; Guntsch's bands require at least 3,000° K., and Pearse's 2,000° K. This last is certainly higher than any temperature, in the ordinary sense, that could be attained in the apparatus used by Pearse, and this suggests that the "temperature" in an arc, as indicated by the energy levels of the molecules, may be much higher than the temperature of the electrodes. If this is conceded, it is seen that the distribution of the recorded bands agrees very closely with that deduced from the wave functions.

On Pearse's plates there are many faint lines for which no analysis has yet been published. Measurements have been made on a number of these, and some of them appear to belong to the (2,3) band of the system (Table 7). This band lies on the inner parabola, and the fact that it is just visible is in fair agreement with its calculated intensity.

Table 7. Lines of (2,3) Band

| | R | | | P | | |
|---|---|---|---|---|---|---|
| | (1) | (2) | (3) | (1) | (2) | (3) |
| 8 | 33106·4 | 33107·6 | 33107·1 | 32966·3 | 32967·2 | 32968·1 |
| 9 | 33087·3 | 33088·4 | — | 32930·4 | 32931·7 | 32932·1 |
| 10 | 33063·2 | 33064·3 | 33065·4 | 32892·0 | 32892·1 | 32892·8 |
| 11 | — | 33039·4 | 33039·5 | 32849·2 | 32850·8 | 32851·0 |
| 12 | 33008·8 | 33009·7 | — | 32805·7 | 32805·7 | 32805·1 |
| 13 | 32976·9 | 32977·9 | 32978·7 | 32757·1 | 32758·1 | 32759·3 |
| 14 | 32942·4 | 32943·1 | 32943·5 | 32707·2 | 32707·6 | 32708·1 |
| 15 | 32904·2 | 32905·6 | 32905·0 | | | |
| 16 | 32864·2 | 32865·4 | 32865·2 | | | |
| 17 | 32820·4 | 32821·0 | 32822·3 | | | |
| 18 | 32774·4 | 32775·3 | — | | | |
| 19 | 32725·9 | 32726·4 | 32726·6 | | | |

(1) $\nu$ calculated from Pearse's data;
(2) $\nu$ calculated from Guntsch's data;
(3) measured values of $\nu$.

There are a few small discrepancies between the calculated intensities and the observed bands :

(1) The calculated intensity of the (3,4) band ($\nu_0 = 32805{\cdot}2$) is low at all temperatures. Yet Guntsch records this band, and even on Pearse's plates a few of the faint lines that have been measured appear to belong to it. Here is apparently a disagreement between calculated and observed intensities.

(2) The (1,6) band ($\nu_0 = 27971{\cdot}4$), which at high temperatures should be noticeably intense, has not been observed. This band, however, would lie in the same region as the (2,7) and (3,8) bands, both of which do appear, and Guntsch states that the lines in this region are crowded, and difficult to identify.

## §8. CONCLUSION

Allowing for the approximations made in the calculations, and for the fact that two independent sets of observations have been used, with a consequent slight discrepancy in the derived constants, there is very close agreement between the calculated and observed distributions of the bands in this spectrum.

## ACKNOWLEDGMENT

The author is indebted to Dr. R. W. B. Pearse for suggesting the subject of this paper, for access to the plates from which his measurements were made, and for help and suggestions throughout.

## REFERENCES

Dunham, J. L., 1932, *Phys. Rev.*, **41**, 721.
Gaydon, A. G., and Pearse, R. W. B., 1939, *Proc. Roy. Soc.* A, **173**, 37.
Guntsch, A., 1934, *Z. Phys.*, **87**, 312; 1939, *Das Bandenspektrum des Magnesium hydrides* (Dissertation).
Morse, P. M., 1929, *Phys. Rev.*, **34**, 57.
Pearse, R. W. B., 1929, *Proc. Roy. Soc.* A, **125**, 157.
Rees, A. L. G., 1947, *Proc. Phys. Soc.*, **59**, 998.

# Nuclear Disintegrations in Photographic Plates exposed to Cosmic Rays under Lead Absorbers

By E. P. GEORGE and A. C. JASON
Birkbeck College, London

*Communicated by G. D. Rochester; MS. received 16th September 1948*

*ABSTRACT.* Ilford Nuclear Research photographic plates have been exposed at the Jungfraujoch, altitude 3,457 metres, under lead screens of various thicknesses up to 28 cm. The intensity of the stars, and its variation with the number of tracks forming them, have been recorded for each thickness of absorber. The absorption curve of the star intensity shows that the range in lead of the radiation causing the stars is $310 \pm 20$ gm/cm². The size distribution is apparently the same under all absorbers.

The intensity and size distribution have also been recorded in similar plates exposed at sea level. The size distribution is again the same as that found for the high altitude plates, but the range in air of the primaries is $150 \pm 7$ gm/cm².

These results are consistent with the generally accepted view that the majority of the stars is caused by neutrons.

## §1. INTRODUCTION

The intensity of the disintegration stars produced in unscreened photographic plates at various heights in the atmosphere has been measured by Stetter and Wambacher (1939), Zdhanov (1939), Lattes, Occhialini and Powell (1947), and Perkins (1947 c). There is general agreement between these authors that the number of stars recorded increases rapidly with altitude. The star intensity is found to vary exponentially with the height according to the relation

$$I = I_0 \exp(-h/R), \qquad \ldots\ldots(1)$$

where $I$ is the star intensity, $h$ the depth from the top of the atmosphere expressed in gm/cm², and $R$, the range of the primaries causing the stars, is of the order of 140 gm/cm².

Very few observations have been made of the absorption of the star-producing radiation in any other material than air. Thus Heitler, Powell and Fertel (1939) compared the intensity of single proton tracks in unscreened plates and plates screened with 13 cm. lead, left at the Jungfraujoch for 230 days. Later, the complete transition curve for single proton tracks up to 12 cm. lead was obtained by Heitler, Powell and Heitler (1940) at the same altitude. More recently, Perkins (1947 c) has recorded the intensity of single proton tracks in photographic plates screened with lead at sea level. All these measurements refer to single tracks and not to stars. The only published paper on the absorption of stars proper is that of Stetter and Wambacher (1944). These authors exposed plates at 2,300 metres altitude, with and without a 10 cm. screen of lead. No significant difference was found either in the number of stars or of single tracks. It seems generally agreed that the absorption of nuclear tracks (single protons or stars) is much less in a given lead absorber than in an equal weight of the atmosphere, though it is apparent that much still remains to be done on the absorption of the star-producing radiation, based on measurements of the stars themselves. We have therefore exposed packets of the new Ilford Nuclear Emulsion plates at the

Jungfraujoch Scientific Station under various lead absorbers up to a maximum of 28 cm. of lead, and under carbon absorbers up to a maximum of 2·5 metres of carbon. Further plates were kept at sea level. In this paper we discuss only the results obtained under the lead absorbers; the results for carbon will be dealt with in a separate communication.

We use the term "intensity of the disintegration stars", or "star intensity" for short, to mean the number of disintegrations recorded in the Nuclear Research plates per cubic centimetre of emulsion per day of exposure. We shall frequently find it necessary to refer to the radiation causing the stars, and for the sake of brevity we shall call it "N-radiation". Finally, by "size distribution" we shall understand a frequency diagram showing the number of stars containing more than $n$ tracks, plotted as a function of $n$.

## § 2. EXPERIMENTAL

The plates used for this experiment were Ilford Nuclear Research, Type $C_2$, 50 microns thick, loaded with boron (borax). They were exposed in the aluminium cabin on the roof of the Scientific Station, Jungfraujoch, Switzerland, height 3,457 metres, average barometric pressure 50 cm. Hg. Care was taken to maintain the roof clear of snow, which was never allowed to remain above 3 inches thick. The cabin was maintained between the temperature limits 17° and 24° c. throughout the exposure.

The screening was arranged as follows. The plates were placed on edge with the plane of the emulsion vertical, and a screen, $t$ cm. thick, built up of lead bricks on the four sides. A roof of lead, $t$ cm. thick, was then placed on top, as shown in Figure 1. Each packet of plates was provided with its own separate screen. When we refer to plates being exposed under a thickness of $t$ cm. lead, we refer to plates screened on five sides to $t$ cm., as shown in Figure 1.

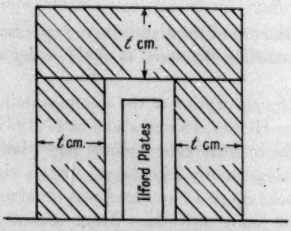


Figure 1. Arrangement of absorbers.

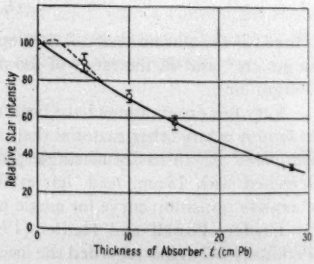


Figure 2. Absorption curve of the star intensity, in lead.

The plates were exposed in two groups. In the first group the exposure was for about 60 days and consisted of plates screened by 0, 15, and 28 cm. of lead. The second was exposed for about 100 days and the plates in it were screened by 0, 5 and 10 cm. of lead. In order to minimize the effects of fading, and any stars that might have been formed while the plates were in transit, they were developed immediately after removal from the lead screen. A further packet of plates was exposed simultaneously in our laboratory on the roof of the Senate House, University of London, for about 100 days.

## § 3. EXPERIMENTAL RESULTS

In recording nuclear disintegration stars in photographic plates care must be taken not to include stars caused by naturally occurring radioactive contamination. To this end we have adopted the definition that a star shall consist of at least three tracks radiating from a common centre, of which at least one track must be longer than 60 microns in the emulsion. From the stars consisting of three tracks we have eliminated those which could be attributed to the scattering of an incident proton in the emulsion.

From the examination of the plates we have obtained (i) the intensity and (ii) the size distribution of the stars formed under lead screens at high altitude, and in unscreened plates at sea level. We discuss the results of these two investigations separately.

### (i) *Absorption Curve of Stars*

The results showing the relative star intensity under the different absorbers are given in Table 1. A total of 2,032 stars has been recorded in 4·7 cm³ of emulsion. In each of the two groups of plates that were exposed for about 60 and 100 days respectively, we included an unscreened packet of plates to serve as a control and thus to enable us to allow for any possible effect of fading. The star intensity in the screened plates of each group, expressed as a percentage of the unscreened control plates in the same group, are given in the last column of the Table.

| | (1) | (2) | (3) | (4) | (5) | (6) | (7) |
|---|---|---|---|---|---|---|---|
| First group* | 64 | 0 | 155 | 0·775 | 440 | 8·8 ±0·4 | 100 |
| | 66 | 15 | 123 | 0·615 | 207 | 5·1 ±0·35 | 58±4 |
| | 65 | 28 | 175 | 0·875 | 170 | 3·0 ±0·23 | 34±2·5 |
| Second group† | 100 | 0 | 118 | 0·59 | 481 | 8·2 ±0·37 | 100 |
| | 110 | 5 | 84 | 0·42 | 339 | 7·4 ±0·4 | 90±5 |
| | 111 | 10 | 89 | 0·445 | 293 | 5·9 ±0·3 | 72±3·5 |
| Sea level | 110 | 0 | 198 | 0·99 | 102 | 0·94±0·10 | |
| Total | .. | .. | .. | 942 | 4·7 | 2032 | |

(1) Exposure (days); (2) thickness of absorber (cm. Pb); (3) area of plate (cm²); (4) volume of emulsion (cm³); (5) stars >3 tracks; (6) stars/cm³/day; (7) star intensity (%).

* Exposed about 60 days at altitude 3,457 m.

† Exposed about 100 days at altitude 3,457 m.

On comparing the intensities in the unscreened plates exposed for the two different times it will be noticed that the number of stars lost due to fading when the exposure is increased from 64 to 100 days is small, of the order of a few per cent. Thus we feel that the errors in the relative star intensity within one group due to fading will be of the order of 1 to 2%, and hence less than the standard deviations of the individual readings. The points in the last column of the Table are plotted in Figure 2. The points can be fitted to an exponential curve, giving for the mean range in lead of the N-radiation, $R_{Pb} = 310 \pm 20$ gm/cm². Our present investigations do not allow us to say at this stage whether there is a Rossi maximum in the star curve at about 2 cm. of lead. We are carrying out a further investigation using small thicknesses of lead in order to settle this point.

At the moment it appears probable that if there is a Rossi maximum in the star curve it is small—an increase of not more than 10 to 20%.

From a comparison of the results in the unscreened plates at high altitude and sea level we may also obtain the range in air, $R_{\text{air}}$ of the N-radiation. The difference in mean pressure between our sea-level laboratory and the Jungfraujoch is 25 cm. Hg or 340 gm/cm². Thus, taking the mean value for the unscreened plates at the high altitude as 8·5 stars per cm³ per day, and at sea level as 0·94, the range in air is given by

$$\frac{8{\cdot}5}{0{\cdot}94} = \exp\left(\frac{340}{R_{\text{air}}}\right), \qquad \ldots\ldots(2)$$

giving $R_{\text{air}} = 150 \pm 7\,\text{gm/cm}^2$, or in other words, the range of the N-radiation in air is almost exactly one half of its range in lead. This result is discussed further below.

(ii) *Size Distribution of Stars*

In Figure 3 we show the size distribution of all the 2,032 stars recorded in this investigation. We will call this the mean size distribution of all stars. Plotting

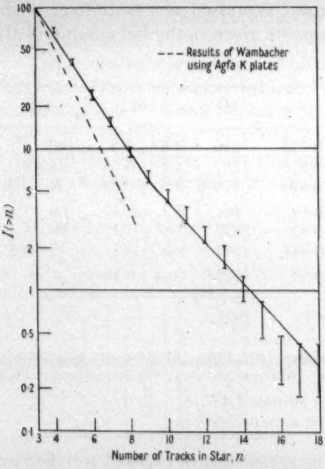


Figure 3. Mean size distribution of all stars.

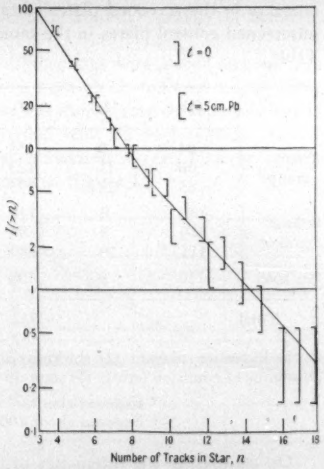


Figure 4 (*a*). Size distribution for $t=0$ and $t=5$ cm. Pb.

log $I(>n)$ against $n$, where $I(>n)$ is the number of stars with more than $n$ tracks, the results appear to lie on a straight line for $3<n<9$, and on another straight line for $n>9$. For the first part of the curve we have

$$I(>n) = I_0 \exp(-0{\cdot}48n) \qquad 3<n<9, \qquad \ldots\ldots(3a)$$

while for the second part we find

$$I(>n) = 0{\cdot}28\, I_0 \exp(-0{\cdot}33n) \qquad n>9. \qquad \ldots\ldots(3b)$$

We do not attach any great significance to the size distribution given by the empirical relations (3 *a*), (3 *b*), since the distribution must in fact be a very complicated relation, depending on the energy spectrum of the N-radiation, the chemical composition of the emulsion etc. For example, the size distribution given by Bagge (1946) obtained from the work of Wambacher in Agfa K plates is also plotted in Figure 3. These results refer to stars of a similar size range to ours, and were obtained at a comparable height, but the number of stars recorded falls off much more rapidly in the Agfa emulsion than was found with the Ilford emulsion.

What we do feel to be of significance, however, is that within the limits of the errors of measurement we find the same size distribution of the stars under all

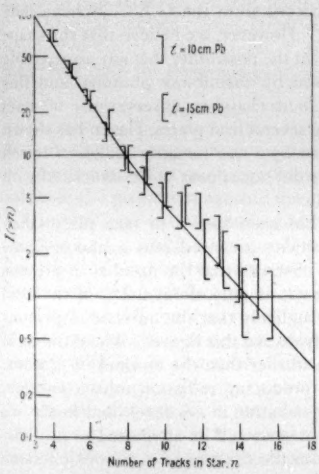


Figure 4 (*b*). Size distribution for $t=10$ and 15 cm. Pb.

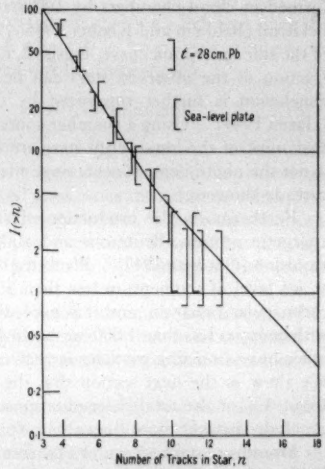


Figure 4 (*c*). Size distribution for $t=28$ cm. Pb and for sea-level plate.

thicknesses of lead and at sea level. This is illustrated in Figures 4 (*a*), (*b*) and (*c*), in which we show separately the points for the size distribution measured under 0 and 5 cm. Pb, 10 and 15 cm. Pb, 28 cm. Pb and at sea level respectively. In each case the curve plotted is the mean size distribution, and it is seen that the individual distributions do not differ from the mean to any significant degree.

## § 4. DISCUSSION OF RESULTS

We may summarize the above results as follows. The range in lead of the N-radiation is found to be $310 \pm 20$ gm/cm., whereas its range in air is $150 \pm 7$ gm/cm$^2$. No significant difference has been detected in the size distribution in plates exposed under lead screens up to a maximum thickness of 28 cm. at Jungfraujoch, or in plates exposed at sea level. In this discussion we shall show that these results support the prevalent view that most of the stars are due to neutrons.

Concerning the range of energies involved, we estimate that the energy required to produce the average star is about 100 Mev., while stars of energies up to and even well above 1,000 Mev. have been observed (Leprince-Ringuet *et al.* 1947).

Now, in the first place, the production of stars by neutrons is possible. Thus Lattes and Occhialini (1947) and C. F. Powell and Occhialini (1947) both give examples of stars which, from a consideration of the resultant momentum and the energy of the tracks, may be attributed without doubt to neutrons. Similarly, W. M. Powell (1947) has reported the production of many stars in the gas of a Wilson chamber bombarded by 90 Mev. neutrons. A photograph showing two of these events is published by Morrison (1948).

Photons, deuterons, alpha-particles and $\sigma$-mesons have also been shown to be capable of causing stars, and their possible contribution to the observed star intensity must be considered. Thus C. F. Powell and Occhialini (1947) have recorded some stars that must be attributed to photons, and stars have also been formed in cloud chambers by 100 Mev. photons from the G.E.C. Schenectady betatron (Baldwin and Klaiber 1946, 1948). However, we believe that the shape of the star absorption curve, Figure 2, rules out the possibility that any appreciable fraction of the observed stars can be caused by cosmic-ray photons, and this conclusion is further supported by the cloud chamber observations of stars (Hazen 1944). Using a chamber containing several lead plates, Hazen has shown that most of the low-energy stars are caused by a non-ionizing radiation which is not the photon component, since the stars did not appear to be associated with cascade showers.

Furthermore, the production of stars has been shown to take place when energetic protons, deuterons and alpha-particles are fired into a photographic emulsion (Gardner 1947). Blackett (1937) observed that the number of protons at sea level of momentum less than 500 Mev/c. is only about 0·2% of the total corpuscular radiation, and it is exceedingly unlikely that the number of protons with energies less than 1,000 Mev. will greatly exceed this figure. The number of other heavy ionizing particles is very much smaller than the number of protons. We show in the next section that the star-producing radiation must constitute about 4% of the total charged corpuscular radiation at sea level, and hence we conclude that not more than about 5% of the stars can be attributed to protons.

Moreover, stars are known to result from the capture of $\sigma$-mesons (Perkins 1947 a, Occhialini and Powell 1947). This interaction always appears to occur when the $\sigma$-meson has come to the end of its range. Of the 2,032 stars observed, the number with more than three tracks produced by $\sigma$-mesons was only 27, or about 1% of the total. After correction for the loss of $\sigma$-mesons due to the small thickness of the emulsion (Lattes, Occhialini and Powell 1947), we find that this upper limit becomes 2%. We have not observed any stars that could be attributed to the capture of a $\sigma$-meson in flight with an energy less than 10 Mev. There remains the possibility that a fraction of the stars may be attributed to $\sigma$-mesons (assumed to experience strong nuclear interactions) with an energy greater than 10 Mev., in which case they would not leave detectable tracks in the emulsion. We cannot rule out this possibility entirely from the available experimental evidence, but we believe the fraction of stars caused in this manner is probably small, for the following reasons. The energy loss of a $\sigma$-meson in traversing our thickest absorber of 28 cm. would be approximately 500 Mev. This would result in a considerable hardening of the emergent $\sigma$-meson spectrum, which one would expect to observe in the size distribution of the stars. Actually no such change was found. Furthermore, we believe that the number of such $\sigma$-mesons that must be assumed to exist is not compatible with the results of cloud chamber investigations at sea level and high altitude.

Let us therefore make the assumption that most of the stars are caused by neutrons with energies within the rough limits indicated above. As a first approximation we make the further assumption that the cross-section for the production of stars is proportional to the nuclear area. In other words, if $r$ is the effective nuclear radius for a nucleus of mass number $A$, then we shall have

$$r = r_0 A^{\frac{1}{3}} \qquad \ldots\ldots (4)$$

with

$$r_0 \simeq 10^{-13} \text{ cm.}, \qquad \ldots\ldots (5)$$

which value is chosen to fit our own range measurements and is reasonably consistent with the cross-section found for the scattering of energetic neutrons by nucleons and with the current theoretical values.

The total nuclear cross-section will be given simply by $a = \pi r^2$, and since the number of nuclei per unit mass, $n$, is $N/A$ where $N$ is Avogadro's number, the mean free path for these energetic neutrons will be, theoretically,

$$l = 1/n\pi r^2 \text{ gm/cm}^2 \quad \text{or} \quad l = A^{\frac{1}{3}}/N\pi r_0^2 \text{ gm/cm}^2. \qquad \ldots\ldots (6)$$

Substituting the value (5) for $r_0$, we obtain $l_{\text{air}} = 130 \text{ gm/cm}^2$, $l_{\text{Pb}} = 310 \text{ gm/cm}^2$.

We do not attach much significance to the agreement between these calculated values of the primary range and the observed ones, since the assumed value (5) of $r_0$ is uncertain to within a factor of two. What perhaps is of more significance is the ratio $l_{\text{Pb}}/l_{\text{air}}$, which is independent of the assumed value of $r_0$ and has the value 2·4, whereas the observed ratio of the ranges of the N-radiation in lead and air has the value $2{\cdot}1 \pm 0{\cdot}2$.

Thus the difference in the range of the N-radiation in air and lead could be due to the existence of an unstable neutral particle, as has been suggested by Perkins (1947 c), or to a stable neutral particle possessing a collision cross-section which is proportional to the nuclear area.

We can likewise fit in the observed constancy of the star size distribution with the assumption that the stars are produced by neutrons, for any change in the size distribution could only be caused by a change in the energy spectrum of the primaries. If, for example, the neutron collision cross-section decreased rapidly with energy in the energy range considered, then we should expect the neutron energy spectrum to become weighted to higher energies as they passed through an absorbing layer, and hence the stars recorded under absorbers would be expected to show a greater preponderance of large stars. That this is not so is shown by the observed constancy of the size distribution, which we believe to be consistent with the expected constancy of the neutron cross-section for energies in excess of a few hundred MeV.

From equation (6) and the known constitution of the Ilford Nuclear Emulsion we obtain a value for the range of the N-radiation in the emulsion :

$$l_{\text{E}} = 1/\Sigma n_A \sigma_A; \qquad l_{\text{E}} = 200 \text{ gm/cm}^2 = 50 \text{ cm.}, \qquad \ldots\ldots (7)$$

where $n_A$ is the number of atoms of atomic number $A$ per unit mass of emission and $\sigma_A$ their cross-section, $\sigma_A = \pi r_0^2 A^{\frac{1}{3}}$. From this range we have been able to form an estimate of the flux of the N-radiation as follows. Let $S$ be the number of N-particles from all directions crossing one cm² per day, and $I$ the number of stars formed in the unscreened emulsion per cm³ per day. Then

$$S/l_{\text{E}} = I. \qquad \ldots\ldots (8)$$

This gives, from (7) and the Table,

$$\left.\begin{aligned} S &= 425/\text{cm}^2/\text{day at Jungfraujoch} \\ &= 12\% \text{ of total charged corpuscular radiation,} \end{aligned}\right\} \quad \ldots\ldots(9a)$$

$$\left.\begin{aligned} S &= 47/\text{cm}^2/\text{day at sea level} \\ &= 4\% \text{ of total charged corpuscular radiation.} \end{aligned}\right\} \quad \ldots\ldots(9b)$$

These intensities are much greater than the intensities of penetrating neutral radiation recorded by Rossi and Regener (1940) and by Jánossy and Rochester (1943). However, it is likely that these authors were recording neutrons of higher energies than the neutrons responsible for the majority of the stars, and it is reasonable to assume that the neutron energy spectrum would show a decrease with increasing neutron energy.

Attempts have been made to measure the flux of fast neutrons using $BF_3$-filled counters (Funfer 1938, Korff and Hamermesh 1946) and photographic plates (Bagge 1946, Morand 1947). We do not feel that the counter measurements are sufficiently developed to enable a useful comparison to be made with our results. The fast neutron fluxes recorded using photographic plates agree reasonably well with the estimates (9). Bagge (1946) calculates the flux of fast neutrons at Jungfraujoch to be about 600 per cm² per day, from the experiments of Schopper (1937, 1939) who observed the increase of single proton tracks in plates covered with thin layers of paraffin. An estimate of the fast neutron flux at sea level has recently been made by Morand (1947). His figure is 43 fast neutrons per cm² per day at sea level. This figure is based on a measurement of single proton tracks observed to start in the emulsion. They are attributed to protons in the emulsion that recoil from fast neutron collisions.

Further evidence on the nature of the N-radiation is provided by the high altitude cloud chamber studies of W. M. Powell (1946) and Hazen (1944), who used chambers containing several lead plates. In the work of W. M. Powell the cloud chamber was counter-controlled, whereas Hazen's chamber was expanded at random. These authors are in agreement that most stars arise from a non-ionizing component of cosmic radiation, which is not to be identified with the photons of the soft component. Since Hazen used no counter-control, his results are probably the more comparable with our observations of stars in photographic plates. We will therefore attempt to correlate our results further with his, which were obtained at an altitude of 3,300 metres.

Hazen observed fifty-eight stars and 19,000 penetrating particles in the same time. The chamber contained eight 0·7 cm. thick plates of lead separated by 2·5 cm. of air. Of the 58 stars, two small ones originated in the gas of the chamber. The particles constituting these two stars had ranges less than 0·7 cm. Pb. This enables us to form an estimate of the number of stars formed in the lead plates giving rise to particles with ranges less than 0·7 cm. Pb. The relative stopping powers of the lead plates to the air spaces is $2{\cdot}6 \times 10^3$ expressed in gm/cm². From our knowledge of the relative ranges of the N-radiation in air and lead ($= 150/310$) we therefore conclude that for every star observed approximately $2/58 \times 2{\cdot}6 \times 10^3 \times 15/31$ or 40 stars containing only short range tracks were not observed. Hazen arrives at a figure of 100 for this factor, but had not allowed for the difference in range of the N-radiation in lead and air. Using our value of the range of the N-radiation in lead, 28 cm., we may now form an estimate of the flux of the N-radiation in Hazen's cloud chamber observations. The total thickness of lead

in the chamber was 5·6 cm., and hence the chance of the formation of a star in the chamber by a primary traversing it was 1/5. Since the number of penetrating particles was 19,000, we will relate the N-particles to twice this number of charged particles since at this altitude the proportions of the hard and soft components are just equal. Hence the number of N-particles expressed as a ratio of the total cosmic-ray flux of charged particles is approximately

$$\frac{\text{N-particles} \times 100}{\text{Total charged cosmic rays}} = \frac{58 \times 40 \times 5 \times 100}{2 \times 19{,}000} = 30\%.$$

This figure is somewhat uncertain owing to the small number of stars originating in the gas of the chamber, and is to be compared with our figure of 12%. It must be borne in mind that our figure will err on the low side because of the number of stars consisting of particles with energies above the limit of detectability in the emulsion. Taken in conjunction with Hazen's conclusion that the initiating particles are predominantly neutrons for the lower energy stars, there seems to be a fair measure of agreement between the conclusions from the cloud chamber and photographic plate observations on stars.

## § 5. CONCLUSION

The absorption curve of Figure 2 shows that the main bulk of the stars cannot be produced by the soft component, and the rapid increase with height shows that they cannot be caused by the penetrating component ($\mu$ mesons), since this component only increases by a factor of 1·7 at the altitude of the measurements. This leaves as alternatives the proton, neutron and $\sigma$-meson components. From the absorption coefficient we find that the required flux of N-particles at sea level must be about 4% of the total corpuscular radiation. The observed rate of protons at sea level (Blackett 1937) shows that not more than about 5% of the stars can be attributed to protons.

This leaves us therefore with the neutrons or $\sigma$-meson components. Our observations on the absorption of the N-radiation in lead and air are consistent with the assumption that the N-particles are neutrons, in agreement with the cloud-chamber evidence, possessing a range proportional to $A^{\frac{1}{3}}$, and energies in the rough limits of 100 MeV. to greater than 1,000 MeV. The size distribution of the stars is found to be the same under all absorbers, and this is again consistent with the prevalent view that the N-rays are neutrons.

The possibility that the stars are also caused to a certain extent by energetic $\sigma$-mesons cannot be ruled out, but it appears probable that the contribution from this component must be small.

*Note added in proof.* Since writing the above, figures for the absorption of the N-radiation in lead and air have been published by G. Bernardini and his collaborators (*Phys. Rev.*, 1948, **74,** 1878) which are in close agreement with our values.

## ACKNOWLEDGMENTS

We wish to thank Professor C. F. Powell and Dr. G. P. S. Occhialini and their group at Bristol for initiating us into the photographic techniques they have perfected. Our thanks are also due to Professor J. D. Bernal for providing us with facilities to do the work and for his continued interest in its progress, and to Professor P. M. S. Blackett for helpful criticism in the preparation of this paper. Many

workers in the Birkbeck Physics Laboratories helped us in the work of scanning the photographic plates, and to these we express our thanks. We are particularly indebted to Mrs. M. H. George for scanning more than half the plates, and to Mr. P. T. Trent for considerable assistance with the scanning technique. We would also like to thank the Director, Professor von Muralt, and the Staff of the Scientific Station, Jungfraujoch, for much assistance during the exposure of the plates. The investigation was made possible by a grant from the Department of Scientific and Industrial Research.

## REFERENCES

BAGGE, E., 1946, *Cosmic Radiation*, ed. W. Heisenberg (New York : Dover Publications).
BALDWIN, G. C., and KLAIBER, G. S., 1946, *Phys. Rev.*, **70**, 259; 1948, *Ibid.*, **73**, 1156.
BLACKETT, P. M. S., 1937, *Proc. Roy. Soc.* A, **159**, 1.
FUNFER, E., 1938, *Z. Phys.*, **111**, 351.
GARDNER, E., 1947, *Phys. Rev.*, **72**, 743A.
HAZEN, W. E., 1944, *Phys. Rev.*, **65**, 67.
HEITLER, W., POWELL, C. F., and FERTEL, G. E. F., 1939, *Nature, Lond.*, **144**, 283.
HEITLER, W., POWELL, C. F., and HEITLER, H., 1940, *Nature, Lond.*, **146**, 65.
JÁNOSSY, L., and ROCHESTER, G. D., 1943, *Proc. Roy. Soc.* A, **181**, 399.
KORFF, S. A., and HAMERMESH, B., 1946, *Phys. Rev.*, **69**, 155.
LATTES, C. M., and OCCHIALINI, G. P. S., 1947, *Nature, Lond.*, **159**, 331.
LATTES, C. M., OCCHIALINI, G. P. S., and POWELL, C. F., 1947, *Nature, Lond.*, **160**, 486.
LEPRINCE-RINGUET, L., *et al.*, 1947, *C.R. Acad. Sci., Paris*, **225**, 1144.
MORAND, M., 1947, *C.R. Acad. Sci. Paris*, **225**, 1146.
MORRISON, P., 1948, *J. Appl. Phys.*, **19**, 311.
OCCHIALINI, G. P. S., and POWELL, C. F., 1947, *Nature, Lond.*, **159**, 186.
PERKINS, D. H., 1947 a, *Nature, Lond.*, **159**, 126; 1947 b, *Ibid.*, **160**, 299; 1947 c, *Ibid.*, **160**, 707.
POWELL, C. F., and OCCHIALINI, G. P. S., 1947, *Nuclear Physics in Photographs* (Oxford : Clarendon Press).
POWELL, W. M., 1946, *Phys. Rev.*, **69**, 385; 1947, *Ibid.*, **72**, 739A.
ROSSI, B., and REGENER, V. H., 1940, *Phys. Rev.*, **58**, 837.
SCHOPPER, E., 1937, *Naturwissenschaften*, **25**, 557; 1939, *Phys. Z.*, **40**, 22.
STETTER, G., and WAMBACHER, H., 1939, *Phys. Z.*, **40**, 702; 1944, *S.B. Akad. Wiss. Wien*, **152**, 1.
ZDHANOV, A. P., 1939, *Akad. Nauk. Odtel. Bull.*, Ser. Phys., **4**, 272.

# Experiments with the Delayed Coincidence Method, including a Search for Short-lived Nuclear Isomers

By D. E. BUNYAN, A. LUNDBY * and D. WALKER
Physics Department, University of Birmingham

*Communicated by M. L. Oliphant; MS. received 9th December* 1948

*ABSTRACT.* The delayed coincidence method has been studied in some detail and employed in a search for short-lived isomers in the product nuclei of $\beta$-emitters. The influence of counter time-lag fluctuations, which determine the short half-life limit in this method, is discussed in relation to the "differential" procedure for recording the delayed coincidences. It is shown that the time lags exhibited by a Geiger-Müller counter are distributed approximately according to a Gaussian law. A differential delayed coincidence recorder has been constructed in which the overall time-lags in the two input channels due to "rise-time" effects have been stabilized. At the coincidence stage of this recorder the quadratic mean deviation in the time-lag difference between the two channels due to "rise-time" effects has been kept as low as $\sim 5 \times 10^{-9}$ sec. Details are given of the experimental procedure used in searching for short-lived isomers. The range of possible half-lives most thoroughly investigated extends from about $3 \times 10^{-7}$ sec. to about $10^{-3}$ sec. for isomeric transitions giving conversion electron energies greater than about 100 kev. Possible improvements in the range of the experiments are discussed. The short-lived isomers of $^{181}$Ta and $^{187}$Re have been confirmed. The half-life of the metastable state in $^{187}$Re has been found to be $(5{\cdot}26 \pm 0{\cdot}12) \times 10^{-7}$ sec. Negative results are reported for 19 isotopes. In particular the metastable states reported by other authors in $^{198}$Hg, $^{141}$Pr, and $^{128}$Te are not confirmed.

The half-life of ThC′ has been found to be $(3{\cdot}04 \pm 0{\cdot}04) \times 10^{-7}$ sec.

## § 1. INTRODUCTION

Since 1946 several nuclear isomers with short decay periods have been discovered by observing delayed coincidences in the radiations from nuclei decaying by $\beta$-emission or K-capture.† This method, using Geiger-Müller counters as detectors, is capable of disclosing, in the product nuclei, metastable levels with half-lives from about $10^{-7}$ to $10^{-2}$ sec. Most of those so far established have half-lives (from $5 \times 10^{-8}$ to $2 \times 10^{-5}$ sec.), transition energies, and internal conversion coefficients consistent with electric octopole or magnetic dipole transitions. This paper discusses delayed coincidence experiments in some detail, including a search for short-lived isomers. Geiger-Müller counters have been used for the detectors.

## § 2. DELAYED COINCIDENCE RECORDERS

The "differential" and "integral" delayed coincidence recorders developed in this laboratory have been described briefly in an earlier paper (Bunyan *et al.* 1948).

### (i) *Integral Recorder*

The integral recorder, developed first and intended to have only the best electronic performance readily achievable, does not exhaust the capabilities of Geiger-Müller counters as regards coincidence resolution. The pulse length in

* Now at the Institutt for Atomenergi, Oslo.

† Bittencourt and Goldhaber (1946), Bowe *et al.* (1948), Bunyan *et al.* (1948), De Benedetti and McGowan (1946, 1947), De Benedetti *et al.* (1948), McGowan and De Benedetti (1948).

channel A (Figure 1) can be varied from approximately $2 \times 10^{-6}$ sec. upwards, while the pulse length in channel B is fixed at about $5 \times 10^{-7}$ sec. The count due to instantaneous coincidences can be assessed by use of an anti-coincidence circuit of short resolving time ($\sim 2 \times 10^{-6}$ sec.), actuated from channel A. This recorder showed no loss of coincidences due to time-lag fluctuations in the Geiger-Müller counters used in our experiments.

### (ii) *Differential Recorder*

In developing the differential recorder, the objective was an electronic performance such that the coincidence resolution would be limited only by the "intrinsic" (electron-transit) time-lags of the Geiger-Müller counters. Care was taken to minimize effects due to fluctuations in the rise-time of the counter anode pulses and small variations in the sensitivity of subsequent trigger circuits

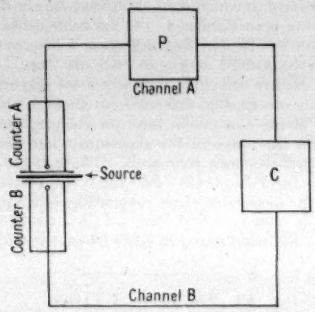


Figure 1. Elements of a delayed coincidence recorder.
P = pulse-delaying circuit (differential recorder) or pulse-lengthening circuit (integral recorder).
C = coincidence stage.

in the apparatus. For this purpose the counter pulses are amplified sufficiently for the subsequent circuits to trigger at one-tenth of the full pulse amplitude. At the inputs to the coincidence stage (Figure 1) the pulse in each of the two channels is $2{\cdot}2 \times 10^{-7}$ sec. in width. The delay introduced in channel A relative to channel B can be varied from $-10^{-6}$ sec. to $+10^{-5}$ sec. in steps of $10^{-7}$ sec.

## § 3. TIME-LAGS IN GEIGER-MÜLLER COUNTERS

### (i) *General*

The "intrinsic" time-lag in a Geiger-Müller counter, i.e. the time of transit of an electron from the region of primary ionization to the region near the anode where an electron avalanche occurs, depends on the type of gas-filling, the gas pressure and the field strength as well as on the radial distance travelled (Den Hartog *et al.* 1947, Sherwin 1948). The intrinsic time-lag can be reduced only by changes in the counter.

The Geiger-Müller counters used in the experiments with the differential recorder described in § 4 (i), (ii) of this paper are cylindrical end-window counters, of cathode diameter 2·5 cm., anode diameter 0·020 cm., cathode length 5·5 cm., anode length 3 cm., and filled with 9 cm. Hg pressure of argon and 1 cm. Hg pressure

of ethyl alcohol. For such a counter the electron transit time from cathode to anode, according to published results (Bradt and Scherrer 1943a, Den Hartog, Muller and Verster 1947), should be approximately $2\times10^{-7}$ sec. Delays due to electron transit time will be statistically distributed when the ionizing particles pass at random distances from the anode, $2\times10^{-7}$ sec. representing the approximate maximum delay. In practice we observe a small fraction of delays, too large to be explained by free electron transit time alone (see § 4 (i)). Sherwin (1948) observes a similar effect, and suggests that it may be due to fluctuations in the time of formation of the positive ion sheath. There may also possibly be a small contribution from electron attachment to form negative ions (cf. Montgomery and Montgomery 1947).

The time-lag between the start of the first electron avalanche in a Geiger counter and the triggering of the associated electronic circuits is dependent both on the counter itself and on the electronic circuits. The rate of rise of the Geiger anode pulse is probably dependent mainly on the velocity of propagation of the discharge along the anode wire (Hill and Dunworth 1946, Alder *et al.* 1947). For the present counters, on this basis, the pulse once started should rise to its peak in about $3\times10^{-7}$ sec., and reach one tenth of the full pulse amplitude in about $3\times10^{-8}$ sec. (cf. § 2 (ii)).

### (ii) *Analysis of Time-lag Effects in the Differential Procedure for Recording Delayed Coincidences*

To determine theoretically the effect of counter time-lags on the coincidence counting rate, we must assume them to follow some distribution law. A Gaussian law, as we shall see, is found to describe the experimental facts closely over a wide range and is used in the following discussion. Bradt and Scherrer (1943a), using a coincidence arrangement with a variable resolving time, have also found agreement with a Gaussian law.

Let us first consider the case in which high energy particles are projected through both Geiger counters or a source which emits radiations in immediate succession is inserted between the counters. Assume a Gaussian distribution of the time lags between the primary ionizing events in a counter and the occurrence of the corresponding pulses at the input of the coincidence stage. Let the Gaussian distribution have a standard deviation $t_0/\sqrt{2}$ for each counter ($t_0$ represents the standard deviation of the difference between the time lags of the two counters). Further, let $\bar{t}_A$ and $\bar{t}_B$ be the average inherent time lags for the two channels (Figure 1) and let the pulses in channel A suffer an additional deliberate delay $t_d$. Let the pulse widths in channels A and B, at the coincidence stage ($\tau_A$, $\tau_B$), be each equal to $\tau$ for simplicity. If a particle causes ionization in counter B at a time $t=0$ the probability of the generated pulse reaching the input of the coincidence stage between $t$ and $t+dt$ is assumed to be given by

$$\frac{1}{t_0\sqrt{\pi}}\exp\left\{-\left(\frac{t-\bar{t}_B}{t_0}\right)^2\right\}dt,$$

and the probability for counter A, when all pulses in this channel are delayed a time $t_d$, is

$$\frac{1}{t_0\sqrt{\pi}}\exp\left\{-\left(\frac{t-\bar{t}_A-t_d}{t_0}\right)^2\right\}dt.$$

The probability that radiations causing ionization simultaneously in both counters shall be recorded as being in "delayed coincidence" is then found to be

$$P(t_d)=\tfrac{1}{2}[\Phi\{(t_d+\tau+\Delta)/t_0\sqrt{2}\}-\Phi\{(t_d-\tau+\Delta)/t_0\sqrt{2}\}], \qquad \ldots\ldots(1)$$

where

$$\Delta=\bar{t}_A-\bar{t}_B, \qquad \text{and} \qquad \Phi(x)=\frac{2}{\sqrt{\pi}}\int_0^x \exp(-z^2)\,dz.$$

Let us next consider the case in which the two radiations are delayed "naturally" with respect to each other, i.e. the half-life of the nucleus formed in the first decay is "finite" ($T_{\frac{1}{2}} \geqslant 10^{-8}$ sec.). We shall assume that the radiation which is emitted first enters counter A, and the following radiation counter B, and that both give rise to discharges in the counters. The probability that the radiations emitted in the formation and the decay of the intermediate nucleus of decay constant $\lambda$ shall be recorded as being in delayed coincidence is then given by the expression

$$\begin{aligned} W(\lambda, t_d)=&\frac{1}{2}\left\{\Phi\left(\frac{t_d+\tau+\Delta}{t_0\sqrt{2}}\right)-\Phi\left(\frac{t_d-\tau+\Delta}{t_0\sqrt{2}}\right)\right\} \\ &+\frac{1}{2}\left[\left\{1+\Phi\left(\frac{t_d-\tau+\Delta}{t_0\sqrt{2}}-\frac{\lambda t_0}{\sqrt{2}}\right)\right\}\exp(\lambda\tau)\right. \\ &\left.-\left\{1+\Phi\left(\frac{t_d+\tau+\Delta}{t_0\sqrt{2}}-\frac{\lambda t_0}{\sqrt{2}}\right)\right\}\exp(-\lambda\tau)\right]\exp(-\lambda t_d-\lambda\Delta+\tfrac{1}{2}\lambda^2 t_0^2). \end{aligned} \qquad \ldots\ldots(2)$$

The first term is equal to $P(t_d)$, and is important only when

$$-(\tau+t_0\sqrt{2}) \lesssim t_d+\Delta \lesssim \tau+t_0\sqrt{2}.$$

The second term contains two factors, of which the first (the expression in the square brackets) is constant for $t_d+\Delta \gg \tau+t_0(\sqrt{2}+\lambda t_0)$. In the latter case the whole expression is equal to Constant $\times \exp(-\lambda t_d)$. Figure 2 gives some examples of the functions $P(t_d)$ and $W(\lambda, t_d)$ for different values of $t_0$ and $\tau$, with $\lambda=2{\cdot}5\times10^6$ sec$^{-1}$. We have put $\Delta=0$ since this transformation results only in a translation of the curves along the $t_d$ axis.

For a given $t_0$ it is seen that in order not to lose too many coincidences $\tau$ must be large compared with $t_0$.

## §4. PERFORMANCE OF THE DIFFERENTIAL RECORDER

Some measurements made with the differential recorder serve to illustrate both the performance of the recorder and the effects discussed in §3.

### (i) *Instantaneous Coincidences*

Using a thin foil coated with $^{60}$Co as a source of instantaneously coincident radiations, the experimental points marked on curve B of Figure 2 were obtained on plotting coincidence rate against the delay of channel A with respect to channel B. (These observed points have all been shifted about $6\times10^{-8}$ sec. to the right in the figure in order to make the centres of the computed and observed curves coincide.) The argon–alcohol counters described in §3 (i) were used, with a thin lead radiator in front of one to increase the efficiency of $\gamma$-detection. The experimental points lie closely along the curve computed from equation (1) with $\tau=2{\cdot}25\times10^{-7}$ sec., and $t_0=10^{-7}$ sec.

For comparison we may note that $(\tau_A + \tau_B)$ as found by random coincidences is equal to $(4{\cdot}37 \pm 0{\cdot}08) \times 10^{-7}$ sec. It should be noted also that, for long delays $t_d$, the observed coincidence rate declines towards zero somewhat more slowly than is consistent with the Gaussian distribution. Thus the fraction of counter time-lags which are larger than can be accounted for simply by the transit time of free electrons (cf. § 3 (i)) is actually somewhat greater than that corresponding to a strict Gaussian distribution.

### (ii) *Stability*

Curve B of Figure 2 can be used to provide a test of the stability of the differential recorder with respect to the time-lag difference between the two channels due to "rise-time" effects. The variation of the coincidence counting rate with

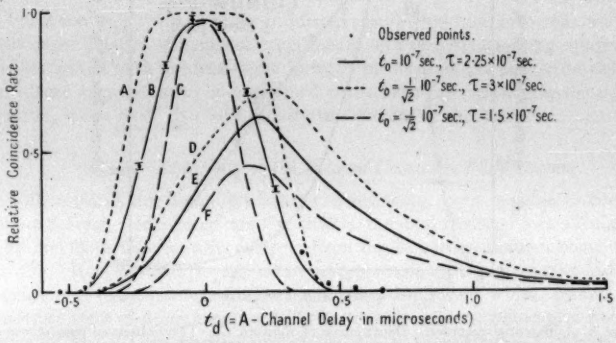


Figure 2. Differential recorder. Variation of coincidence rate with A-channel delay ($t_d$). Curves A, B, C are of $P(t_d)$ computed from equation (1), and curves D, E, F are of $W(\lambda, t_d)$ computed from equation (2), using $\lambda = 2{\cdot}5 \times 10^6$ sec$^{-1}$ and the indicated values of $t_0$ and $\tau$. For the observed points see § 4 (i).

a change in delay setting ($t_d$) is very rapid at that setting where the rate is reduced to half its maximum (the coincidence rate changes by about 85% for a change of $10^{-7}$ sec. in $t_d$), and thus the stability of the recorder can be assessed by observing coincidence rate fluctuations in prolonged operation at this setting. The fluctuations observed in a series of readings during a continuous test run of twenty hours corresponded to a quadratic mean deviation in the time-lag difference between the two channels due to "rise-time" effects of approximately $5 \times 10^{-9}$ sec.

In a test of the stability against fluctuations in the anode voltage of the Geiger-Müller tubes, the change in coincidence counting rate observed for a deliberate change of 25 volts in the working voltage on either tube corresponded to a change in the effective mean time-lag of approximately $2 \times 10^{-8}$ sec. This is reasonable if one considers the variation with overvoltage of the velocity of propagation of a discharge along the anode wire of a counter (Hill and Dunworth 1946).

### (iii) *Half-life of Thorium C′*

As a further test of the performance of the differential recorder, the decay period of ThC′ was redetermined. The source was an active deposit from radio-thorium (ThB + ThC).

The experimental points on curve A, Figure 3, show the variation of the observed coincidence rate with A-channel delay ($t_d$), using the Th(B + C) source on a platinum foil between the counters. The counter in channel A was a Geiger-Müller $\beta$-counter of the type described in § 3 (i). In channel B a proportional counter was used, operated in the high proportional region. This counter was an end-window type, 2·7 cm. in diameter and 5 cm. long. The window was a 2·3 mg/cm² Al foil, and the counter was filled with a helium–alcohol mixture at

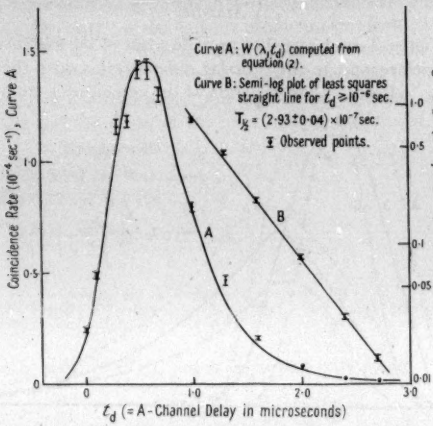
Curve A: $W(\lambda, t_d)$ computed from equation (2).
Curve B: Semi-log plot of least squares straight line for $t_d \geq 10^{-6}$ sec.
$T_{\frac{1}{2}} = (2{\cdot}93 \pm 0{\cdot}04) \times 10^{-7}$ sec.
I Observed points.
Coincidence Rate ($10^{-4}$ sec$^{-1}$), Curve A
Coincidence Rate ($10^{-4}$ sec$^{-1}$), Curve B
$t_d$ (= A-Channel Delay in microseconds)

Figure 3. Differential recorder. Decay curve of thorium C′. (The observed coincidence rates have been corrected for the decay of the Th(B+C) source.)

atmospheric pressure, the alcohol pressure being 1 cm. Hg. Owing to the lower electron mobility in this counter as compared with that in channel A the magnitude of the time-lag fluctuations is larger. Curve A (Figure 3) is of the function $W(\lambda, t_d)$ computed from equation (2) using $\lambda = 2{\cdot}37 \times 10^6$ sec$^{-1}$ ($T_{\frac{1}{2}} = 2{\cdot}93 \times 10^{-7}$ sec.), $\tau = 2{\cdot}25 \times 10^{-7}$ sec., and $t_0 = 2 \times 10^{-7}$ sec.

The experimental points on curve B, Figure 3, are for A-channel delays equal to or greater than $10^{-6}$ sec. and fit a half-life for ThC′ of $(2{\cdot}93 \pm 0{\cdot}04) \times 10^{-7}$ sec. The error in the calibration (only approximate) of the delay lines may be as great as 10%.* The half-life of ThC′ was first estimated by Dunworth (1939) as $(3 \pm 1) \times 10^{-7}$ sec. Recent values are those of Bradt and Scherrer (1943 b), $T_{\frac{1}{2}} = (2{\cdot}6 \pm 0{\cdot}4) \times 10^{-7}$ sec.; and of Hill (1948), $T_{\frac{1}{2}} = (3{\cdot}00 \pm 0{\cdot}15) \times 10^{-7}$ sec.

## § 5. DETAILS OF EXPERIMENTAL PROCEDURE USED IN SEARCHING FOR SHORT-LIVED ISOMERS

### (i) *Preparation of Sources*

Substances to be activated have been obtained as fine, chemically pure and chemically stable powders (the element or its oxide) and sealed into silica tubes for neutron irradiation in the small pile at the Atomic Energy Research Establishment, Harwell. Specific activities of the desired $\beta$-emitters of $10^6$ or more disintegrations

* *Footnote added in proof.* The delay lines have since been calibrated using a crystal-controlled pulse generator, and we find $(3{\cdot}04 \pm 0{\cdot}04) \times 10^{-7}$ sec. for the absolute half-life of ThC′.

per second per gramme have been obtained. In preparing sources for coincidence experiments, some of the irradiated powder of grain size less than approximately $10\mu$ has been glued, using a layer of cellulose nitrate lacquer of less than 1 mg/cm² thickness, to one side of an aluminium foil of about 2 mg/cm² thickness. (At $10\mu$ grain size and a density of 15 gm/cm³, self-absorption in the grains would reduce the intensity of a 50 kev. electron component to approximately one-tenth of that in the absence of self-absorption, and the intensity of a 100 kev. component to approximately one-half.)

In mounting the foil between the two counters (Figure 1) the source side faced counter B.

### (ii) *Checking the Decay Periods of the β-Emitters*

The decay in activity of all the irradiated samples has been followed, independently of the delayed coincidence experiments, on a separate counting equipment. This has served both to identify the isotopes involved and to enable the delayed coincidence experiment to be performed at the most favourable time for a given $\beta$-emitter, when more than one activity was present in the sample.

### (iii) *The Sensitivity of the Delayed Coincidence Experiments*

With most of the $\beta$-emitters examined it has not been possible to detect a genuine delayed coincidence rate $C_g$: that is, the total recorded coincidence rate $C_t$ has not been significantly different from the computed random coincidence rate $C_r$. It is possible to assess, by an approximate argument, the order of magnitude of the minimum fraction $\phi$ of the $\beta$-transitions which, leading to a metastable state of decay constant $\lambda$ in the product nucleus, would give rise to a detectable $C_g$. This smallest detectable $C_g$ is $C_g=(\phi N_A)\epsilon_{B2}f$, where it is assumed that the counting rate $N_A$ in counter A is due only to $\beta$-particles, where $\epsilon_{B2}$ = net efficiency of counter B for the delayed radiation; and, for the *differential recorder*, $f\simeq\exp(-\lambda t_1)[1-\exp\{-\lambda(\tau_A+\tau_B)\}]$, where $t_1$ is the maximum intrinsic counter time-lag difference occurring with appreciable frequency. The corresponding minimum delay setting at which no instantaneous coincidences can be recorded through the influence of counter time lags is $(t_1+\tau_B)$. This is the most favourable setting for detecting delayed coincidences. $\tau_A$, $\tau_B$ are the pulse lengths in the two channels at the coincidence stage. For the *integral recorder*, $f=\exp(-\lambda\tau_0).\exp\{-\lambda(\tau_A-\tau_0)\}$, where $\tau_0$ is the length of the anti-coincidence pulse used to suppress instantaneous coincidences ($t_1\leqslant\tau_0<\tau_A$, and $\tau_B\ll\tau_A$).

The individual counting rates in counters A and B being $N_A$ and $N_B$, the random coincidence rate is computed from $C_r=N_AN_B(\tau_A+\tau_B)$.* The relative error in $C_r$ is therefore the relative error $\eta$ in $(\tau_A+\tau_B)$ †, since $N_A$, $N_B$ can be measured with a high statistical accuracy. The relative error in the total coincidence rate $C_t$ is, on simple statistical reasoning, $1/(C_tt)^{\frac{1}{2}}$, where $t$ is the counting time, and this, since $C_r\simeq C_t$ in the limit of small $C_g$, is $1/(C_rt)^{\frac{1}{2}}$.

$C_g$ is obtained by subtracting $C_r$ from $C_t$, and hence, to be detected, must exceed the absolute error in either. Thus the minimum detectable $C_g$ is either $\eta N_AN_B(\tau_A+\tau_B)$ or $(C_r/t)^{\frac{1}{2}}=\{N_AN_B(\tau_A+\tau_B)/t\}^{\frac{1}{2}}$, whichever is greater. Once either error has been reduced to its practical limit, decrease of the other below the

* Strictly for the integral recorder, $C_r=N_AN_B(\tau_A-\tau_0)$.

† The relative error in $(\tau_A+\tau_B)$ is determined partly by its stability.

same magnitude brings little improvement, so that at the optimum the error in $C_r$ should be roughly equal to the error in $C_t$. At this limit

$$(C_g)_{\min} = \phi N_A \epsilon_{B2} f \simeq \eta N_A N_B (\tau_A + \tau_B) \simeq \{N_A N_B (\tau_A + \tau_B)/t_c\}^{\frac{1}{2}},$$

where $t_c$ is the counting time required to reach this condition.

From this

$$\phi = \frac{(N_B/N_A)^{\frac{1}{2}}}{\epsilon_{B2}} \left(\frac{\tau_A + \tau_B}{t_c}\right)^{\frac{1}{2}} \frac{1}{f} \qquad \ldots\ldots (3)$$

at the optimum given by

$$(N_A N_B)^{\frac{1}{2}} t_c^{\frac{1}{2}} = \frac{1}{\eta(\tau_A + \tau_B)^{\frac{1}{2}}} \qquad (N_A \sim N_B \text{ in general}).$$

When searching for delayed coincidences, we have at all times observed the conditions for optimum $\phi$, using $t_c \sim 24$ hours.

(iv) *Quantitative Estimate of Detection Sensitivity* $\phi$

In searching for delayed coincidences with the *integral recorder* we have used for counter B a 2·5 cm. diameter Geiger counter with a mica end-window 2·5 mg/cm² thick, and filled with helium–alcohol mixture to atmospheric pressure. For a window thickness of 2·5 mg/cm² the limiting electron energy is 35 kev.* The source was less than $\frac{1}{2}$ cm. from the counter, and $\epsilon_{B2} > 0{\cdot}05$ for a sufficiently energetic transition completely internally converted. (Rather strong internal conversion usually accompanies isomeric transitions.) The anti-coincidence resolving time was approximately $2 \times 10^{-6}$ sec., the A channel pulse length, for a simple test for delayed transitions, set at about $10^{-5}$ sec. and $\eta = 0{\cdot}02$. Under these conditions, and with $N_A = N_B$, $\epsilon_{B2} \geqslant 0{\cdot}05$ and $t_c = 24$ hours, equation (3) gives the following maximum values of $\phi$ for the half-lives indicated:

| $T_{\frac{1}{2}}$ (sec.) | $3 \times 10^{-7}$ | $5 \times 10^{-7}$ | $10^{-6}$ | $10^{-5}$ | $10^{-4}$ | $10^{-3}$ | $10^{-2}$ |
|---|---|---|---|---|---|---|---|
| $\phi$ | $3 \times 10^{-2}$ | $4 \times 10^{-3}$ | $9 \times 10^{-4}$ | $6 \times 10^{-4}$ | $3 \times 10^{-3}$ | $3 \times 10^{-2}$ | $3 \times 10^{-1}$ |

$\phi$ will increase inversely as the internal conversion coefficient when this is less than 1. For soft electrons ($\lesssim$100 kev.) self-absorption (§ 5 (i)) and window absorption must be also taken into account.

With the *differential recorder* ($\eta = 0{\cdot}05$), if the helium counters described in the preceding paragraph are used, the simple test of operating at a fixed delay setting ($t_1 + \tau_B$) (§ 5 (iii)) gives no striking gain in sensitivity over the integral recorder for very short half-lives. The intrinsic time-lags of the atmospheric pressure helium counter are excessive, and the window thickness (7 mg/cm²) necessary with a reduced pressure argon counter of the type described in § 3 (i) decreases the efficiency of detection of soft electron components. The values of $\phi$ given in the preceding paragraph may therefore be taken in conjunction with all the negative results listed in § 6 (ii).

A numerical example of the foregoing considerations was obtained by delayed coincidence measurements on tungsten using the integral recorder with $(\tau_A - \tau_0) = 1{\cdot}90 \times 10^{-6}$ sec. About 10% of the $\beta$-particles from $^{187}$W (half-life 24 hours) are followed by delayed conversion electrons from the decay of a

* Counter A has been either similar to counter B, or one of the argon–alcohol counters described in § 3 (i) with a window thickness of 7 mg/cm² (limiting electron energy 75 kev.).

metastable level in $^{187}$Re, of half-life $5 \times 10^{-7}$ sec. (De Benedetti and McGowan 1947). No delayed coincidences have been observed in the radiations from $^{185}$W (half-life 77 days). In a source made of neutron-activated tungsten, containing both these isotopes, a genuine delayed coincidence rate $C_g$ of $(1{\cdot}68 \pm 0{\cdot}78) \times 10^{-4}$ counts per second was still detected when the $\beta$-radiation leading to delayed electron emission was only 0·17% of the total $\beta$-radiation from the sample. The value of $\phi$ computed for this case was 0·2%.

### (v) *Improvement of Sensitivity*

For half-lives less than approximately $10^{-7}$ sec. the sensitivity of the differential recorder can be increased by using Geiger-Müller counters with smaller intrinsic time-lags, that is, effectively, argon–alcohol counters of smaller cathode diameter. For half-lives of approximately $10^{-2}$ to $10^{-1}$ sec. it is an advantage with the integral recorder to use a correspondingly large $\tau_A$. The background counting rates may then become important but could be reduced by lead shielding. With $\tau_A \sim 10^{-3}$ sec. in the present recorder $\eta > 0{\cdot}02$, and this could be improved. Over the whole range of operation of both recorders the sensitivity of the technique would be improved by careful preparation of very thin sources (e.g. by electro-deposition) to avoid self-absorption of low energy electrons, and by placing the sources inside the counters to eliminate window absorption and improve the geometrical conditions.

For future work the possibilities offered by new methods of particle detection (e.g. scintillation methods employing photo-multipliers) should not be overlooked. Reduced detector time-lags as well as improved efficiency of $\gamma$-detection (cf. the effect of $\epsilon_{B2}$ in equation (3)) are both important.

## §6. EXPERIMENTAL RESULTS*

### (i) *Positive Results*

$^{181}_{73}$Ta: First found by De Benedetti and McGowan (1946), the metastable level (half-life $(20{\cdot}1 \pm 0{\cdot}7) \times 10^{-6}$ sec.) in $^{181}_{73}$Ta following the $\beta$-decay of $^{181}_{72}$Hf (half-life 48 days) was investigated by us and a report on the decay scheme given in an earlier paper (Bunyan *et al.* 1948). Beneš *et al.* (1948) report in their examination of $^{181}_{72}$Hf with a $\beta$-ray spectrometer that L-conversion of the soft $\gamma$-ray following the metastable level in $^{181}_{73}$Ta is greater than K-conversion. Thus the value of 200 kev. which we gave for the energy of this transition, obtained by adding the K-binding energy (70 kev.) to the energy of the conversion electrons (130 kev.) as found by absorption, is too high. Beneš *et al.* give the energy of the $\gamma$-ray as 128 kev. from their spectrograph measurements.

$^{187}_{75}$Re: $\beta$-decay of $^{187}_{74}$W (24 hours half-life) leads to a metastable level in $^{187}$Re, first reported by De Benedetti and McGowan (1947). Figure 4 shows the results of one of our experimental runs with the differential recorder using a $^{187}$W source. Counter A was one of the 2·5 cm. diameter argon counters and counter B one of the 2·5 cm. diameter atmospheric pressure helium counters (§5 (iv)). Curve A, Figure 4, illustrates the type of record obtained when both instantaneous and delayed coincidences originate from the same source. Curve B, Figure 4, is a semi-logarithmic plot of the coincidence rate for A-channel delays $\geqslant 7 \times 10^{-7}$ sec.

* Since the work described here was completed, De Benedetti and McGowan (1948) have published an account of a search for short-lived isomers.

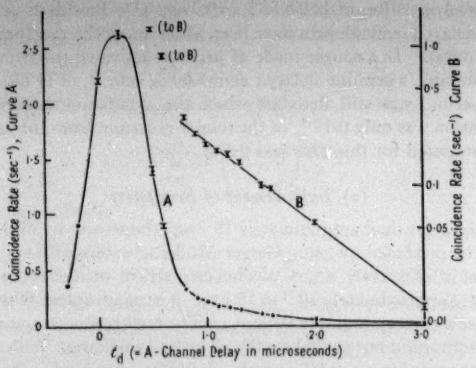


Figure 4. Differential recorder. Decay curve of the metastable state in $^{187}$Re. (The observed coincidence rates have been corrected for the decay of the $^{187}$W source.)

| β-emitter | Half-life | β-emitter | Half-life | β-emitter | Half-life |
|---|---|---|---|---|---|
| $^{204}_{81}$Tl | 3·5 years | $^{192}_{77}$Ir | 70 days | $^{177}_{71}$Lu | 6·6 days |
| $^{203,\ 205}_{80}$Hg | 51·5 days | $^{191}_{76}$Os | 30 hours | $^{143}_{59}$Pr | 13·5 days |
| $^{198}_{79}$Au | 2·7 days | $^{193}_{76}$Os | 17 days | $^{143}_{58}$Ce | 36 hours |
| $^{199}_{79}$Au | 3·3 days | $^{188}_{75}$Re | 18 hours | $^{141}_{58}$Ce | 30 days |
| $^{197}_{78}$Pt | 18 hours | $^{186}_{75}$Re | 90 hours | $^{124}_{51}$Sb | 60 days |
| $^{197}_{78}$Pt | 3·3 days | $^{185}_{74}$W | 77 days | | |
| $^{194}_{77}$Ir | 20·7 hours | $^{182}_{73}$Ta | 117 days | | |

NOTES

**$^{198}$Au**. Madansky and Wiedenbeck (1947) reported a metastable level in $^{198}_{80}$Hg, following β-decay of $^{198}$Au, whose existence neither Mandeville and Scherb (1948) nor ourselves have been able to confirm.

**$^{199}$Au** was formed by the decay of $^{199}$Pt (31 m.). The sensitivity of our tests in this case is $\frac{1}{6}$ that implied from § 5 (iii), (iv), since radiation from 3·3 days $^{197}$Pt present in the source tended to mask possible delayed coincidences.

**$^{141}$Ce**. A metastable state of half-life $(7\pm2)\times10^{-5}$ sec. in $^{141}$Pr following β-decay of $^{141}$Ce was reported by Hirzel *et al.* (1947). In measurements with the integral recorder over a range of integrating pulse lengths ($\tau_A$) up to several times $10^{-4}$ sec.,* and with the source deposited on the inside of the window of counter B no delayed coincidences were detected by us.

**$^{143}$Ce** and **$^{143}$Pr** were also tested in the same fashion as $^{141}$Ce. In the case of $^{143}$Pr, owing to the masking effect from the β-radiations of $^{141}$Ce present in the source, the sensitivity of the test was about $\frac{1}{5}$ that implied by § 5 (iii), (iv).

**$^{124}$Sb**. Hirzel *et al.* (1947) also reported a metastable state of half-life $(1\cdot2\pm0\cdot4)\times10^{-3}$ sec. in $^{124}$Te formed by β-decay of $^{124}$Sb. Tests were made over a range of integrating pulse lengths up to several times $10^{-4}$ sec.,* but none with the source inside the counter. No delayed coincidences were observed.

**$^{185}$Re** (product nucleus of $^{185}$W) is possibly of some interest since it possesses the same spin (5/2) and the same magnetic moment (3·3 nuclear magnetons) as $^{187}$Re, which has a metastable state. In spite of our negative results, $^{185}$Re may have a metastable state outside the reach of the present method, or any method so far tried with this isotope.

* The upper limit of detectable isomeric half-lives is about 10 times that for $\tau_A=10^{-5}$ sec

The value of the half-life, computed by the method of least squares from the values for A-channel delays $\geqslant 10^{-8}$ sec., is $(5{\cdot}03 \pm 0{\cdot}12) \times 10^{-7}$ sec. The probable error given is derived purely from statistical considerations; the error due to the uncertainty in the calibration of the delay lines may be as great as 10%.*

### (ii) *Negative Results*

The following $\beta$-emitters were examined without evidence being obtained of metastable levels in the product nuclei. Except with the Ce and Pr activities, when the source was placed on the inside of the window of counter B,† radiation entering counter B had to pass through a window 2·5 mg/cm² thick (limiting electron energy 35 kev.). The $\beta$-counter, counter A, had either a 7 mg/cm² or a 2·5 mg/cm² window. The sensitivity of our tests is discussed in § 5 (iii), (iv).

ACKNOWLEDGMENTS

We should like to thank Professor M. L. Oliphant and Professor P. B. Moon for the interest they have shown in this work.

REFERENCES

Alder, F., Baldinger, E., Huber, P., and Metzger, F., 1947, *Helv. Phys. Acta*, **20**, 73.
Beneš, J., Ghosh, A., Hedgran, A., and Hole, N., 1948, *Nature, Lond.*, **162**, 261.
Bittencourt, P. T., and Goldhaber, M., 1946, *Phys. Rev.*, **70**, 780.
Bowe, J. C., Goldhaber, M., Hill, R. D., Meyerhoff, W. E., and Sala, O., 1948, *Phys. Rev.*, **73**, 1219.
Bradt, H., and Scherrer, P., 1943 a, *Helv. Phys. Acta*, **16**, 251; 1943 b, *Ibid.*, 259.
Bunyan, D. E., Lundby, A., Ward, A. H., and Walker, D., 1948, *Proc. Phys. Soc.*, **61**, 300.
De Benedetti, S., and McGowan, F. K., 1946, *Phys. Rev.*, **70**, 569; 1947, *Ibid.*, **71**, 380; 1948, *Ibid.*, **74**, 728.
De Benedetti, S., McGowan, F. K., and Francis, J. E., 1948, *Phys. Rev.*, **73**, 1404.
Den Hartog, H., Muller, F. A., and Verster, N. F., 1947, *Physica*, **13**, 251.
Dunworth, J. V., 1939, *Nature, Lond.*, **144**, 152.
Hill, J. M., 1948, *Proc. Camb. Phil. Soc.*, **44**, 440.
Hill, J. M., and Dunworth, J. V., 1946, *Nature, Lond.*, **158**, 833.
Hirzel, O., Stoll, P., and Wäffler, H., 1947, *Helv. Phys. Acta*, **20**, 241.
McGowan, F. K., and De Benedetti, S., 1948, *Bull. Amer. Phys. Soc.*, **23**, No. 2, 42.
Madansky, L., and Wiedenbeck, M. L., 1947, *Phys. Rev.*, **72**, 185.
Mandeville, C. E., and Scherb, M. V., 1948, *Phys. Rev.*, **73**, 634.
Montgomery, C. G., and Montgomery, D. D., 1947, *Rev. Sci. Instrum.*, **18**, 411.
Sherwin, C. W., 1948, *Rev. Sci. Instrum.*, **19**, 111.

* *Footnote added in proof.* The delay lines have since been calibrated using a crystal-controlled pulse generator, and we find $(5{\cdot}26 \pm 0{\cdot}12) \times 10^{-7}$ sec. for the absolute half-life of the metastable state in $^{187}$Re.

† The geometrical efficiency of counter B $\sim 0{\cdot}5$ in these cases.

# DISCUSSION

on paper by F. C. CHAMPION and R. R. ROY entitled "The Scattering of Fast $\beta$-Particles through Large Angles by Nitrogen Nuclei" (*Proc. Phys. Soc.*, 1948, **61**, 532).

Professor N. FEATHER (Edinburgh). Comparison of experiment with theory obviously involves averaging over a finite range of $\beta$-particle energy, not only because the theoretical result is energy-dependent, but also because the distribution of scattering points over the chosen scattering volume will be different for particles of different energy (due to differences in extent of magnetic deflection) and because the penetrability of the counters will also be different. Equally obviously, there is a limit to the amount of computation which is profitable. I should like to enquire whether the authors think that their correction terms omit any serious effect of energy-dependence.

Dr. W. T. DAVIES (Clarendon Laboratory, Oxford). It may be of interest to mention some unpublished results by Dr. C. O'Ceallaigh and myself on the nuclear scattering of electrons in air. The work was carried out in Cambridge and London before the war; the conventional cloud chamber method was used, and the energy range investigated was from 1 to nearly 3 MEV.

In a measured track length of nearly 90 metres, out of a total length of about 210 metres we found eight cases of elastic scattering through more than 50° where 1 or 2 were to be expected. In view of the smallness of these numbers the significance of our results is open to doubt, although I should point out that the divergence from theory becomes even greater when a correction is applied for the restricted observational solid angle. A fact of possibly greater significance, however, is that scattering with an apparent energy loss exceeding 0·2 of the incident energy was found by us to occur with roughly the same frequency as elastic scattering for angles of scattering greater than 20°, whereas according to an estimate by Mott it should be of order 1/100 as frequent (Mott and Massey, *The Theory of Atomic Collisions* (Oxford : University Press), p. 272).

AUTHORS' reply. We do not consider that our correction terms omit any serious effect arising from energy-dependence. The corrections involved have been the subject of previous examination on several occasions for particles from the same source, and the energy distribution between $\beta=0{\cdot}84$ to $0{\cdot}94$, in the scattering volume considered, is well known experimentally. While the penetrability of the counters will be different, as the critic suggests, it will not make a serious contribution over the range of energy considered. Such possible errors and others being taken into account, together with those arising from probability fluctuations, would indicate an accuracy of $\pm 20\%$.

We have pointed out that our experimental apparatus is unsuitable in its present form for the examination of inelastic collisions. In earlier experiments with nitrogen and a non-controlled cloud chamber, very few examples of inelastic collisions were found. However, the energy region just below 1 MEV., investigated by the authors, is considerably less than that used by Dr. Davies. It is just possible that inelastic collision may increase rapidly with energy above about 1 MEV., but the recent results of Van de Graaff *et al.*, which claim extreme accuracy, show no indication of this.

---

# LETTERS TO THE EDITOR

## Infra-Red Photoconductivity in Layers of Tellurium and Arsenic

Evaporated layers of tellurium have been prepared which exhibit marked photoconductivity at low temperatures when irradiated by wavelengths in the near infra-red, although previous investigators have concluded that this element is not photosensitive (Coblentz 1918, Brown and MacMahon 1929).

The films were deposited on graphite electrodes on the inner walls of small pyrex Dewar flasks. For a tellurium layer, about one milligram of material was inserted into the flask, which was then evacuated to a pressure of less than $10^{-6}$ mm. of Hg, as recorded on an ionization gauge. The material was distilled on to the outer wall of the vessel and purified by heating just below the evaporation temperature for periods of one to several hours. Finally the layer was distilled on to the electrodes.

Taking the thickness of the films as $10^{-4}$ cm., specific resistances of about 1 ohm cm. were obtained at room temperature, and 10–20 ohm cm. at liquid oxygen temperature. The response times of the layers (i.e. time required for signal to decay to $1/e$ after illumination by a pulse of light) were in the range 500 to 1,000 microseconds. The spectral distribution of sensitivity was measured for one layer which was made in an envelope with a thin "bubble" window of pyrex for which the absorption would be negligible over the range of wavelengths concerned. The results are shown in Figure 1, where the relative signal

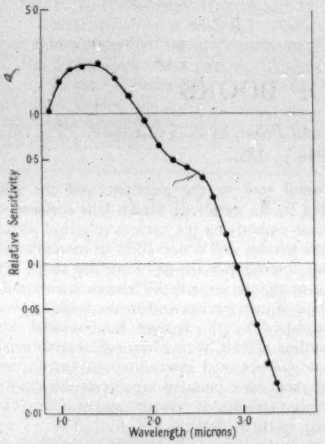


Figure 1. Spectral sensitivity of tellurium layer at 90° K.

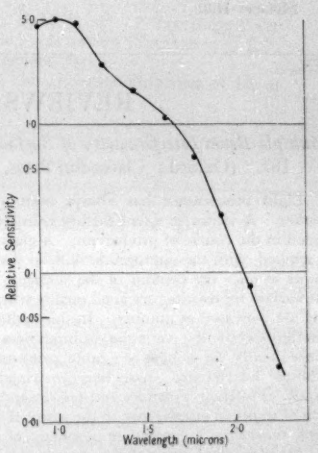


Figure 2. Spectral sensitivity of arsenic layer at room temperature.

output (referred to constant incident energy) is plotted on a logarithmic scale. It may be seen that a rapid exponential fall of sensitivity commences at 2·7 $\mu$. The most sensitive tellurium cell so far made gave a signal equal to r.m.s. noise in 1 c/s. bandwidth for an incident energy of $10^{-9}$ watts from a source at roughly 2,000° K., using an interruption rate of 800 c/s.

Banks, Neuman and Schoenfeld, working at the Polytechnic Research and Development Company, Brooklyn, New York, under a contract with the U.S. Office of Naval Research, have independently observed photoconductivity in evaporated and sputtered films of tellurium.

Layers of arsenic showing slight photoconductivity have also been prepared. It is to be noted that whereas for tellurium the effect was appreciable only at low temperatures, for arsenic strong cooling ruined the layer.

Some preliminary measurements have been made on layers of arsenic prepared by techniques similar to those used for tellurium. It is, however, much more difficult to produce mechanically stable layers of this material, and so far only one layer with sensitivity adequate for measuring the spectral response curve has been made. Even in this case very low resolution had to be used in order to get sufficient energy on the layer. The curve is shown in Figure 2. As the wavelength is increased, an exponential fall off begins at about 1·7 $\mu$.

This layer had a specific resistance of $10^6$ ohm cm. (approx.) and a response time of $10^{-3}$ seconds. The arsenic layers had a grey metallic appearance at room temperature, but cooling with liquid oxygen converted them to the red allotropic form, and the photosensitivity disappeared.

I am indebted to the Ministry of Supply for permission to carry out this work at Cambridge and to Dr. Banks for communicating to me (through Dr. G. B. B. M. Sutherland) the results referred to above, before publication.

Department of Colloid Science,
Cambridge.
5th January 1949.

T. S. Moss.

Coblentz, W. W., 1918, *Bull. Nat. Bur. Stand., Wash.*, **14**, 591.
Brown, F. C., and MacMahon, A. M., 1929. *International Critical Tables*, **6** (New York: McGraw-Hill).

---

# REVIEWS OF BOOKS

*Multiple-Beam Interferometry of Surfaces and Films*, by S. Tolansky. Pp. viii + 187. (Oxford: Clarendon Press, 1948.) 18*s*.

Light interference has always been a useful tool to the scientist and the glass worker. A visitor to a lens factory is impressed by the ease with which lens surfaces are tested in the course of production. A glass gauge embodying the correct spherical surface is applied, with the appropriate skill, to the lens surface and observation in mercury light shows at once the contour of the surface. One interference fringe of regular shape over the surface represents very good quality whereas in an inferior lens the fringes are irregular and are increased in number. In this application of interference and in the usual types of interferometers the variation in brightness produced by the fringes is sinusoidal and consequently the fringes are quite fuzzy in outline. By silvering the surfaces to create multiple interference, sharp line-like fringes can be obtained instead of the broad fuzzy bands. Professor Tolansky and his research workers have pursued vigorously the application of multiple interference to the study of surface markings in crystals, metals etc. This book represents a convenient summary of their work to date.

An immediate result of the sharpened fringes is the increased accuracy with which the topographical features can be measured. In extremely favourable cases an accuracy of 3 A. is quoted as having been attained. This is indeed remarkable for a system using ordinary light.

The general tone and outlook of the book is that of practical application of this particular optical tool. There is a brief clear theoretical treatment of multiple interference, careful distinction being drawn between the different kinds of fringes and their localization. The bulk of the book, however, is concerned with the examination of surfaces of mica, quartz, metals etc., with results illustrated by numerous photographs. The possibilities of the method will be of interest to those who are concerned in the topography of surfaces, surface finishes etc., and there are also the possible applications to the measurement of small distances and movements of small amplitude.

A chapter is devoted to interference colour filters. This type of filter would be a very useful addition indeed to the customary range of absorbing filters, but at present they remain surprisingly difficult to obtain commercially. R. D.

# CONTENTS FOR SECTION B


| | PAGE |
|---|---|
| Dr. G. LIEBMANN. Measured Properties of Strong "Unipotential" Electron Lenses | 213 |
| Dr. A. B. BHATIA. On the Electrical Properties of Cold Worked Iron Carbon Alloys | 229 |
| Mr. M. K. I. ARAFA. A Calculation of the Solubility Limits of the Copper–Silver System | 238 |
| Mr. J. P. ROBERTS. Mechanical Breakdown of a Non-Metallic Polycrystalline Material Observed by Reflected Light Microscopy | 248 |
| Mr. K. GOLDSMITH and Dr. J. IBALL. The Measurement of the Rheological Properties of Visco-plastic Substances | 251 |
| Mr. J. CRANK and Miss M. E. HENRY. A Comparison of the Rates of Conditioning by Different Methods | 257 |
| Letter to the Editor: | |
| Mr. R. B. R.-SHERSBY-HARVIE and Mr. L. B. MULLETT. A Travelling Wave Linear Accelerator with R.F. Power Feedback, and an Observation of R.F. Absorption by Gas in Presence of a Magnetic Field | 270 |
| Dr. JOHN LAMB and Mr. A. TURNEY. The Dielectric Properties of Ice at 1·25 cm. Wavelength | 272 |
| Reviews of Books | 273 |
| Contents for Section A | 275 |
| Abstracts for Section A | 275 |


# ABSTRACTS FOR SECTION B

*Measured Properties of Strong "Unipotential" Electron Lenses*, by G. LIEBMANN.


*ABSTRACT.* The Hartmann test and the "knife-edge" method for the determination of lens constants are described as applied to the investigation of electrostatic "unipotential" lenses. The results of measurements on a number of such lenses are presented graphically.

It is shown that the curvature of the principal surfaces plays an important part and that it is, therefore, necessary to distinguish between longitudinal spherical aberration and difference of zonal focal lengths. Up to about half the lens diameter, primary spherical aberration only is noticeable in most cases. The dimensionless spherical aberration constant $S$ can be approximately represented, over a wide range of modifications of lens design or lens potentials, by the formula $S=K_1(f/D)^2$, $f$ being the focal length and $D$ the internal diameter of the centre electrode of the lens. $K_1$ is a constant of the order of 10 for the lenses investigated without stops limiting the axial length of the field, and of the order of 20 for lenses incorporating such stops. In the case of one specially constructed lens, good agreement is found with calculations by Ramberg. In an experimental unipotential lens for which the diverging parts of the electrostatic field were removed, the spherical aberration is as low as in magnetic lenses of comparable dimensions.


*On the Electrical Properties of Cold Worked Iron Carbon Alloys*, by A. B. BHATIA.


*ABSTRACT.* The change on "aging" in the electrical properties of cold worked iron–carbon alloys of low concentration is investigated theoretically. During the process of "aging", the carbon atoms diffuse into the dislocations, thus forming rows of atoms. The electrical resistance due to scattering of electrons *by these rows of carbon atoms* is expressed in terms of the scattering power of a single carbon atom dissolved in the iron lattice, and hence in terms of the resistance of the same number of randomly distributed carbon atoms. It is found that this change depends on the wavelength of the electrons at the Fermi surface. This wavelength is determined by the effective number of free electrons, and with a reasonable value of about 0·6 electrons per atom for iron, the agreement with the observed diminution in resistance is satisfactory.

Alternatively, one can use the calculations to determine both the number of free electrons in iron and the number of dislocations in the specimen at different degrees of hardening, from the observed changes in the electrical resistance and thermoelectric power of the specimen.

*A Calculation of the Solubility Limits of the Copper–Silver System*, by M. K. I. ARAFA.

*ABSTRACT.* A calculation is made of the change in the energy of a monovalent metal when one of its atoms is replaced by an atom of a different monovalent metal, not necessarily of the same atomic volume. From a knowledge of this energy the heat of solution can be determined and thereby, through the usual thermodynamic relations, also the solubility limits. Numerical calculations have been carried out for the copper–silver system and the theory shows in this case the existence of narrow solubility limits, in agreement with the known phase diagram. The theoretical values of the heats of solution are compared with those required to give the observed solubility limits.

*Mechanical Breakdown of a Non-Metallic Polycrystalline Material Observed by Reflected Light Microscopy*, by J. P. ROBERTS.

*ABSTRACT.* A study of fracturesin a well-sintered polycrystalline aggregate of corundum crystals has shown that the strengths of the crystals and the crystal-boundaries are approximately equal. Reflected light microscopy was employed and the usefulness of this method of examination has been established.

*The Measurement of the Rheological Properties of Visco-plastic Substances*, by K. GOLDSMITH and J. IBALL.

*ABSTRACT.* A torsion device is described in which a small and decreasing stress is exerted on the visco-plastic substance by means of a blade attached to a torsion wire. A modification of the Scott Blair-Nutting equation is suggested to account for the variation of both stress and strain with time and a " firmness intensity factor " of the substance is calculated, by means of the modified equation, from the observed relation between blade deflection and time. The apparatus has been used to study the properties of milk curds.

*A Comparison of the Rates of Conditioning by Different Methods*, by J. CRANK and M. E. HENRY.

*ABSTRACT.* Four methods of conditioning a sample of material to a prescribed liquid or vapour content are examined mathematically. The " two-stage method " of conditioning leads to considerably shorter conditioning times than the other methods provided it is carried out in a certain way, and information presented in graphical form in this paper shows how to obtain the maximum advantage in practice. The necessary equations are developed for both a plane sheet and a cylinder, and the corresponding problem in heat flow is mentioned.

---

## CORRIGENDA

" Nuclear Disintegrations in Photographic Plates exposed to Cosmic Rays under Lead Absorbers ", by E. P. GEORGE and A. C. JASON (*Proc. Phys. Soc.* A, 1949, **62**, 243).

Pages 250–251, last paragraph of §4. The figures " 19,000 ", occurring three times, should read " 9,000 ".

The percentage stated in the subsequent formula should read " 60 per cent " and not " 30 per cent ".